Supplementary Materials

Li et al., An integrin checkpoint restrains myeloid cells in immune-mediated glomerular disease

Sections:

Materials and Methods

Supplementary Figures S1 to S23

Supplementary Tables S1 to S8

Supplementary References

Materials and Methods

Reagents and antibodies

The small molecule CD11b agonist compound ONT01 was a gift from Allosite Therapeutics (Miami, FL). Bovine serum albumin (BSA) was from Sigma (St. Louis, MI). Non-fat milk was obtained from BioRad (Hercules, CA). PCR reagents were obtained from New England Biolabs Inc (Beverly, MA). All cell culture reagents were purchased from Thermo Fisher Corp (San Diego, CA). LPS (cat# tlrl-eklps), Pam2 (cat# tlrl-pm2s-1), Pam3 (cat# tlrl-pms), PMA (cat# tlrl-pma), polyI:C (cat# tlrl-plc) and CpG (cat# tlrl-2216) were purchased from Invivogen (San Diego, CA). Human and mouse recombinant cytokines and ELISA kits were purchased from R&D Systems and were declared by the manufacturer to contain <0.1 ng of LPS per μg of protein. The following primary antibodies for western blot were purchased from Cell Signaling Technologies (Danvers, MA): Phospho IKK-α/β (cat# 2078), IKK-β (cat# 8943), Phospho p65/NF-kB (cat# 3036), MyD88 (cat# 4283), GAPDH (cat# 2118), Phospho IRF3 (cat# 4947), IRF3 (cat# 4302), Phospho IRF7 (cat# 14767), Phospho c-Cbl (cat# 8869), c-Cbl (cat# 8447), Phospho Src (cat# 6943), and Src (cat# 2108). Other antibodies used were anti-rabbit IgG-HRP conjugate (cat# W4011, Promega, Madison, WI), anti-mouse IgG-HRP conjugate (cat# W4021, Promega, Madison, WI), NF-kB (cat# 16502, Abcam, Cambridge, MA), and IRF7 (cat# PA5-20280, Thermo Scientific, Waltham, MA). Antibodies used for immunofluorescence experiments were as follows: WT1 (cat# SC-192, Santa Cruz), synaptopodin (cat# SC-21537, Santa Cruz), activated β1 (cat# 553715, BD Biosciences) C3 (cat# GC3-90F-Z, ICL, Inc.) or IgG (cat# A11029, Thermofisher Scientific). The following antibodies for flow cytometry experiments were purchased from Biolegend (San Diego, CA): APC/Cyanine7 anti-mouse CD45 (cat# 103115), PE anti-mouse Ly-6G (cat# 127607), APC anti-mouse Ly-6C (cat# 128015), FITC anti-mouse Gr-1 (cat# 108406), APC anti-mouse/human CD11b (cat# 101212), APC/Cyanine7 anti-mouse CD45 (cat# 103116), Alexa Fluor 488 anti-mouse/human CD11b (cat# 101217), Brilliant Violet 650 anti-mouse/human CD11b (cat#101259), PE/Cyanine7 anti-mouse F4/80 Antibody (cat#123113), Brilliant Violet 711™ anti-mouse Ly-6G Antibody (cat#127643),

APC/Cyanine7 anti-mouse CD45 Antibody (cat#103115), APC anti-mouse CD3 Antibody (cat#100236), PE/Dazzle™ 594 anti-mouse CD4 Antibody (cat#100565), PerCP/Cyanine5.5 anti-mouse CD8a Antibody (cat#100734), and PE anti-mouse CD68 Antibody (cat#137014). The following antibodies are from Thermo Fisher: MHC Class II (cat# 56-5321-82), CD45R (B220) Monoclonal Antibody (cat# 48-0452-82). The following antibodies for flow cytometry were purchased from BD Biosciences: BD Pharmingen FITC Rat Anti-Mouse Ly-6G and Ly-6C (cat# 553127), BD Horizon PE-CF594 Rat Anti-CD11b Antibody (cat# 562287). LIVE/DEAD Fixable Aqua Dead Cell Stain Kit was purchased from Thermofisher Scientific (cat# L34966). Compensation beads were from Invitrogen (cat#01-2222-42), and live/dead compensation beads were from Invitrogen (cat#A10628).

meQTLnet (myeloid trans-eQTL regulatory linkage network) framework

To map the trans-regulatory effects of a genetic locus and to establish a generalizable framework for detecting conformational checkpoints, we developed meQTLnet, a locus-anchored approach for discovering how disease-associated variants reshape gene-regulatory networks in myeloid cells. The framework involves six steps. First step is *haplotype partitioning*, where locus variants are grouped into LD-defined blocks, for example, separating a coding haplotype (rs1143679, R77H) from a regulatory haplotype (rs3087796) in *ITGAM*. Second step is to map any *trans-eQTLs* and identify genome-wide trans-eQTL targets of each coding variant/cluster in various trans-eQTL atlases (eQTLGen Phase 1 and Phase 2) and the target count is tested against a matched–minor-allele-frequency permutation null. Third step is to examine *cis-pQTL*, where each cluster's cis effect on its own protein product is mapped in a plasma proteomic atlas (UKB) and classified as abundance-null or abundance-driving. Fourth step is to make a *conformational-signature call*, where a coding variant locus is called positive when at least one cluster is simultaneously null for its own cis-pQTL and drives an enriched trans program - the defining signature of a variant that modulates downstream transcription without altering its own protein level. Fifth step is to examine any *directionally coherent networks or programs* via cross-locus convergence analysis on a curated disease-associated gene set for any module based trans-eQTL effects and directional

consistency, to identify effects on signaling programs. Sixth step is to examine *cluster-module orthogonality* by testing the trans programs of distinct clusters by correlating their trans-target effect sizes, establishing whether the coding-linked and regulatory-linked arms act on non-overlapping modules. The framework returns a binary conformational-signature call, the cluster-assigned trans-gene list, that, together, define the trans-regulated program downstream of the locus.

To map this program for *ITGAM*, we queried trans-eQTL associations for variants at the *ITGAM* locus in two eQTLGen datasets: Phase 1 (N = 31,684, whole blood; ~10,000 trait-associated SNPs tested in trans) and Phase 2 (N = 43,301; genome-wide trans-eQTL scan) (1, 2). We retained trans-eQTL associations at FDR < 0.05 for any *ITGAM* locus variant (rs1143679/R77H and linked variants at $r^2 \geq 0.5$), prioritizing transcripts with the strongest association across the locus, and extended each top trans-target to a complete module by testing all locus variants against genes in the curated 21-gene type-I interferon signature (IFN21) (3). To resolve LD clusters, we grouped locus variants by linkage-disequilibrium block ($r^2 \geq 0.9$). This segregated two clusters with opposing functional signatures: coding variants (led by rs1143679/R77H) drove coherent interferon-stimulated gene (ISG) upregulation, whereas regulatory variants (led by rs3087796) produced heterogeneous, thematically incoherent trans-effects—establishing conformation, not abundance, as the functional axis. The retained IFN21 reanalysis used Benjamini-Hochberg correction across 21 exact-rs1143679 tests, separately from the published source-wide trans-eQTL FDR.

We then mapped cis-regulatory effects for each haplotype to establish their dissociation from the trans signal. Testing plasma CD11b abundance in 51,031 UK Biobank participants, the coding haplotype (rs1143679) showed no cis-effect on abundance (P = 0.629), whereas the regulatory haplotype (rs3087796) drove a strong cis-effect; we confirmed the cis-null property of R77H against GTEx (4) whole-blood cis-eQTL data, finding no credible cis-eQTL for *ITGAM* across tissues. We validated the trans signal at the protein layer by querying trans-pQTL associations in UK Biobank Olink (N = 51,031; 1,472 proteins) and the Koprulu plasma proteomic meta-analysis (N = 78,000) (5) retaining proteins modulated by the coding haplotype at FDR < 0.10 and focusing on innate-immune/myeloid-specific

proteins (BST2, SIGLEC1, MSR1, CD163, FCN1, CXCL10, CCL8, LGALS9) and integrin-complex components (ITGB2).

To characterize LD between the two haplotypes, we computed LD between the lead variants rs1143679 (coding) and rs3087796 (regulatory) in 1000 Genomes phase 3 EUR (Ensembl REST) (6) obtaining $r^2 = 0.07$ with $D' \approx 1.0$; the low r^2 reflects the allele-frequency offset between the leads and governs their separability. R77H was absent from the plasma CD11b cis-abundance credible set, and the regulatory lead returned no ISG trans-eQTL at FDR < 0.05, placing the two signals in non-overlapping credible sets. Although R77H sits on the common regulatory background ($D' \approx 1.0$), the interferon program segregated with R77H rather than with that background: carriers of the regulatory allele lacking R77H—the much larger group—showed no ISG trans-eQTL, whereas the cis-abundance signal tracked the regulatory allele independently of R77H. The two effects are therefore attributable to distinct variants—receptor conformation versus receptor abundance—rather than to a single shared haplotype.
To assess cross-locus convergence, we curated 21 independent SLE/immune-disease-associated SNPs and tested their trans-eQTL effects on the *ITGAM*-regulated ISG module, quantifying convergence as the fraction of SNPs regulating each target with directional consistency. To localize the trans signal to myeloid cells, we analyzed single-cell eQTL data (OneK1K (7), GSE149050) and queried sorted-cell expression atlases (DICE (8), BLUEPRINT (9)), assessing whether *ITGAM* trans-targets are most highly expressed in myeloid relative to lymphoid populations. The following statistical thresholds were applied: Bonferroni correction for trans-eQTL discovery ($\alpha = 0.05$ / ~20,000 genes $= 2.5 \times 10^{-6}$); FDR < 0.05 for Phase-1 trans scans and FDR < 0.10 for pQTLs; and an LD inclusion threshold of $r^2 \geq 0.5$.
Approximate conditional analyses of ITGAM cis-eQTL and plasma trans-pQTL associations used harmonized summary statistics and external linkage-disequilibrium estimates, adjusting for rs3087796 alone or together with rs11865830. Conditional trans-pQTL P values were adjusted using the Benjamini–Hochberg method.

eQTLGen Population-Level QTL Screen for the architecture

To identify common coding variants that anchor a distant trans-regulatory program with no cis effect on its own gene across the genome, we used eQTLGen Phase 1 (2) and Phase 2 (1) whole-blood trans-eQTL datasets as discovery backbone. Phase 1 contained 3,853 unique SNPs from 31,684 individuals and 59,786 significant trans-eQTL associations and the Phase 2 contained 110,431 total cis, trans, and intermediate associations. Protein-altering trans anchors were identified by ensemble rsID-based VEP annotation requiring direct host-gene transcript consequences including missense, splice, stop, frameshift, in-frame indel, start-loss, or other protein-altering terms for common variants (minor-allele frequency ≥ 1%, gnomAD). We also used plasma trans-pQTLs (UKB with 21,528 fine-mapped trans associations (10) and the Koprulu et al. plasma proteomics meta-analysis of UKB and SCALLOP with 19,698 fine-mapped trans associations (5)). Union of common-missense trans-anchors across the four substrate scans yielded 1,086 variant-by-substrate observations corresponding to 819 unique lead variants. Collapsing these variants to their host genes (107 genes carried two or more independent common-missense anchors) and merging two genes catalogued under both a legacy and a current symbol (*HMHA1*/*ARHGAP45*, *KIAA1551*/*RESF1*) defined a catalogue of 676 candidate trans-anchoring loci. We then filtered for own-gene cis-null (the trans signal is not attributable to cis-mediation of the host's own gene) to obtain an own-cis-null set of 217 genes. Because a trans signal can be produced indirectly by a cis effect that the discovery scan leaves unresolved, we tested every member against GTEx v8 DAP-G fine-mapping across tissues, requiring that the lead variant fall outside the credible set of both its host gene and any neighboring gene (maximum posterior inclusion probability below 0.1 in every tissue). We used credible-set membership rather than marginal significance because a variant in linkage disequilibrium with a causal cis-eQTL shows a marginal cis association without itself being causal. Twenty-nine members carried a credibly causal cis signal on this criterion and were removed. A further eight lead variants were absent from GTEx v8 and could not be tested; these were retained, having already met the cis-null criterion in eQTLGen and in both plasma proteomic scans. This yielded a de-confounded own cis-null set of 188 members. As an autoimmune-GWAS comparison can be confounded by immune expression itself, we required each member's host protein to be expressed in at least one

sorted immune lineage, using the Human Protein Atlas (11) immune-cell RNA dataset (maximum normalized expression ≥ 1 nTPM across the 18 sorted lineages, total PBMC excluded). This gate removed proteins detected in blood only because they are made by non-immune cells (e.g. erythroid, platelet, or secreted/hepatic proteins), leaving 143 members. To remove members whose lead variant is a cis-pQTL for their own protein (an abundance effect) we analyzed cis-pQTL in UKB (10) and removed *CSF2*, *IL7R* and *TLR1* to obtain 140 protein-dose-clean members. We finally required each member to anchor at least two trans-eQTLs at genome-wide significance, positing that a lone trans hit was treated as insufficient evidence of a program, and removed any gene with non-distal trans-eQTLs (associations whose lead lies within 1–5 Mb of the target gene). This provided us with a final family of 80 members.

To check for disease associations, we mapped each member's lead variant and host gene against the GWAS Catalog. To check that the members' substitutions are tolerated, conformation- or activity-altering changes rather than destabilizing ones, we computed, for the 80 family (each carrying a parseable single missense substitution) and the immune-expression-matched null used for the disease comparison (n = 308, of which 55 carry a single parseable missense substitution scored here), the Grantham distance (12) of each substitution and its AlphaMissense pathogenicity (13). We report the fraction of conservative (Grantham < 100) and likely-benign (AlphaMissense < 0.34) substitutions, repeated with CpG-accessible arginine substitutions removed to control for CpG mutational accessibility. Family variants are predominantly conservative and predicted-tolerated and this skew survives CpG removal, but the family is not distinguishable from the immune-matched null on the conservative and tolerated fractions, consistent with the class being defined by its regulatory architecture rather than by a shared chemistry.

Human LN gene expression data acquisition and preprocessing

Single-cell RNA sequencing (scRNA-Seq) data from the Accelerating Medicines Partnership (AMP) Systemic Lupus Erythematosus (SLE) Consortium Phase II dataset (14) was acquired from the ARK Portal (https://arkportal.synapse.org/) under the applicable data-use terms. This work was supported by the Accelerating Medicines Partnership Rheumatoid Arthritis and Systemic Lupus Erythematosus

(AMP RA/SLE) Program. AMP is a public-private partnership created to develop new ways of identifying and validating promising biological targets for diagnostics and drug development. Funding for AMP was provided through grants from the National Institutes of Health (UH2-AR067676, UH2-AR067677, UH2-AR067679, UH2-AR067681, UH2-AR067685, UH2-AR067688, UH2-AR067689, UH2-AR067690, UH2-AR067691, UH2-AR067694, and UM2-AR067678).

The analysis used AMP kidney scRNA-seq data from lupus nephritis and healthy control kidney biopsy samples, AMP blood PBMC CITE-seq data from paired donors, AMP TOPMed-imputed genotyping data, and donor clinical and renal-response covariates. Population-structure covariates were generated for this analysis from genome-wide AMP genotype data using ancestry principal components and exported as donor-level covariates. For the CosMx spatial plots (15), the cell identities and glomerular context were taken from the published childhood-onset LN CosMx 1000-plex annotations and plotted in native spatial coordinates. Dataset source was Danaher et al. 2024, Childhood-onset lupus nephritis is characterized by complex interactions between kidney stroma and infiltrating immune cells, Zenodo. 2024. doi: 10.5281/zenodo.13964258.

AMP Kidney scRNA-seq Processing

Kidney scRNA-seq cell count matrices were joined to sample metadata and clinical covariates by barcode, sample, subject, and visit identifiers. Quality control (QC) was performed to remove patients with less than 200 evaluable cells in their samples, as well as low-quality cells based on gene feature detection (<200 genes or >3500 genes), and high mitochondrial transcript proportions (>50%). The initial QC layer retained 465,242 cells. The annotated kidney figure layer contained 465,043 cells from 184 donors and was used for UMAP visualization and donor-level summaries (155 LN donors and 29 healthy control donors). Primary donor comparisons excluded repeat-biopsy rows and used one observation per participant.

Kidney scRNA-seq counts were log-normalized in Seurat v5 (16). The top 3000 highly variable genes were selected, principal component analysis was performed, and the first 30 PCs were used for

integration and embedding. Subject-layer reciprocal PCA was used for integration. Graph-based clustering was performed at resolution 1.0, and UMAP was used for visualization.

Kidney Cell Typing and Analysis

Kidney clusters were annotated using marker gene expression and kidney immune-cell biology. Myeloid cells were defined from monocyte, macrophage, and dendritic-cell enriched immune clusters with support from markers including *ITGAM, LST1, FCER1G, CD14, FCN1, S100A8, S100A9, ITGAX, HLA-DRA, C1QA,* and *C1QB*. CD11b/*ITGAM*-positive myeloid cells were annotated myeloid cells with *ITGAM* expression greater than zero.

Age-associated B cells were identified within B-cell enriched clusters using *ITGAX, TBX21, FCRL5, ZEB2, SOX5, FGR, FCRL4, CXCR3,* and *CD86* expression, with *JCHAIN, MZB1, TNFRSF17,* and *XBP1* used to separate plasma-cell programs. Donor-level CD11b/*ITGAM*-positive myeloid fraction was calculated as *ITGAM*-positive myeloid cells divided by all kidney cells for that donor. Donor-level ABC fraction was calculated as ABC cells divided by all kidney cells for that donor.

Canonical IFN and NF-κB Scoring

Canonical IFN was defined as the Yao 21-gene type I interferon signature (3). The NF-κB module was defined from MSigDB Hallmark TNFA/NF-kB leading-edge genes (17). For donor-level kidney and blood summaries, expression was aggregated to donor-compartment pseudobulk log1p(CPM). Within each compartment, each measured module gene was converted to a robust z score across donors by subtracting the median, dividing by IQR/1.349, clipped to -3 to 3, and averaged across measured module genes for a final unitless module score. The combined IFN/NF-κB heatmap used standardized module-derived traces for donor ordering but displayed gene-level myeloid expression values.

The NF-κB score used the union of kidney bulk and myeloid Hallmark leading edges, after pathway assignment and overlap removal and requiring availability in both kidney and blood exports (125

genes). The IFN21 genes were EPSTI1, HERC5, IFI27, IFI44, IFI44L, IFI6, IFIT1, IFIT3, ISG15, LAMP3, LY6E, MX1, OAS1, OAS2, OAS3, PARP9, PLSCR1, RSAD2, RTP4, SIGLEC1, USP18. The NF-κB scoring genes were AREG, ATF3, BCL2A1, BCL3, BHLHE40, BIRC3, BTG1, BTG2, CCL2, CCL20, CCL4, CCL5, CCNL1, CCRL2, CD69, CD80, CD83, CDKN1A, CEBPB, CEBPD, CSF1, CXCL10, CXCL11, CXCL2, CXCL3, DENND5A, DUSP1, DUSP2, DUSP4, DUSP5, EDN1, EGR1, EGR2, EGR3, ETS2, FOS, FOSL2, FUT4, G0S2, GADD45B, GCH1, GEM, GPR183, HBEGF, ICAM1, IER2, IER3, IER5, IFIH1, IFIT2, IFNGR2, IL15RA, IL1B, IL6, INHBA, IRF1, IRS2, JAG1, JUNB, KDM6B, KLF2, KLF4, KLF6, KYNU, LDLR, LITAF, MAFF, MAP2K3, MARCKS, MCL1, MXD1, MYC, NAMPT, NFIL3, NFKB2, NFKBIE, NINJ1, NR4A1, NR4A2, NR4A3, OLR1, PDE4B, PHLDA2, PLAU, PLAUR, PLEK, PLK2, PLPP3, PPP1R15A, PTGER4, PTGS2, PTPRE, RCAN1, REL, RELB, RHOB, RIPK2, SAT1, SDC4, SERPINB8, SERPINE1, SGK1, SLC16A6, SLC2A3, SLC2A6, SMAD3, SOCS3, SOD2, SPHK1, SQSTM1, TAP1, TGIF1, TIPARP, TNC, TNF, TNFAIP3, TNFAIP6, TRAF1, TRIB1, TSC22D1, TUBB2A, VEGFA, YRDC, ZC3H12A, ZFP36.

For the paired AMP kidney-blood heatmap, donors with paired kidney and blood myeloid summaries were grouped by paired bulk Canonical IFN score tertile. The heatmap included 117 paired LN donors, with 39 donors in each tertile. Heatmap expression values were row-standardized z scores clipped to the plotting range. Other donor-level boxplots were not restricted to this paired kidney-blood set. Each used all donors eligible for the plotted tissue compartment, genotype, or response contrast, and minimum cell-support rule.

Pseudobulk Expression

Donor pseudobulk expression was calculated by aggregating counts within the relevant donor cell compartment, normalizing to the RNA library size for that donor compartment, multiplying by one million, and applying log1p transformation. *CCL2* kidney bulk expression and *PLAUR* kidney myeloid expression are reported as donor-level pseudobulk log1p(CPM). The R77H myeloid expression background panel used median donor-level kidney myeloid pseudobulk log1p(CPM) for each gene in LN

R77H carriers and non-carriers, with Canonical IFN genes highlighted. *IRF7*/*PLAUR* double-positive cells were defined as annotated kidney myeloid cells with both *IRF7* expression greater than zero and *PLAUR* expression greater than zero. The donor-level *IRF7*/*PLAUR* double-positive fraction was calculated as double-positive myeloid cells divided by all annotated myeloid cells for that donor. The unadjusted donor-weighted odds ratio for IRF7/PLAUR double-positive cells compared 32 carriers with 95 non-carriers, with a bootstrap 95% confidence interval. The odds ratio was [pC/(1-pC)]/[pN/(1-pN)], where pC and pN are the equally weighted mean donor fractions in carriers and non-carriers. Whole donors were resampled with replacement separately within genotype groups (20,000 replicates); the 95% interval used the exponentiated 2.5th and 97.5th percentiles of bootstrap log odds ratios. This analysis used all 127 typed LN donors with a nonempty target compartment.

Genotyping and Ancestry Covariates

AMP genotypes were obtained from TOPMed-imputed hg38 PLINK .bed, .bim, and .fam files containing 723 AMP samples, including 175 scRNA-linked donors. ITGAM R77H/rs1143679 was reconciled by rsID, genomic coordinate, and allele orientation; the hg38 coordinate used for PLINK-backed extraction was 16:31265490:G:A. Donor genotype tables included rs1143679 GT, alternate-allele count ALT_CT, DS, explicit R77H carrier status, *ITGAM* haplotype fields, and ancestry PCs.

Downstream R77H carrier status used a conservative dosage-resolved patient-level call. Genotypes were assigned only when dosage evidence supported a clear alternate-allele count, while ambiguous or repeated-sample-discordant calls were retained as untyped. In the 175 donor-matched genotype data, 33 donors were classified as R77H carriers, 116 as non-carriers, and 26 as unresolved or untyped with dosage available. Ancestry PCs were generated with PLINK2 from genome-wide autosomal variants; 20 PCs were generated, and genotype models used ancestry covariates up to PC5.

AMP Blood PBMC CITE-seq Processing

AMP blood PBMC CITE-seq analyses used quality-controlled GEX raw counts, ADT raw counts, cell metadata, sample metadata, and feature annotation tables. RNA and ADT values were normalized as log1p counts per million using full-library denominators before target-marker summarization. The blood PBMC donor layer used for donor-level summaries included 145 donor samples and 349,176 cells: 122 Case samples, 20 Control samples, and 3 samples with combined Case;Repeat labels.

Blood Myeloid cells were derived from AMP broad Monocyte and DC labels. Classical monocytes were identified using *CD14, S100A8, S100A9, LILRB1, CTSS, CD14 protein,* and *ITGAM*, compared against *FCGR3A, LST1, SAT1, IFITM3*. pDCs were identified using *IL3RA, GZMB, JCHAIN, TCF4, IRF7*. cDC/myeloid DCs were identified using *FCER1A, CLEC10A, CD1C, ITGAX,* and *ITGAX* protein. ABC-like B cells were identified using F*CRL5, TBX21, ITGAX, CD27*, compared with naive and memory B-cell marker programs.

CosMx Spatial Kidney Analysis

LN CosMx spatial kidney analysis used the cleaned segmented-cell CosMx object and bundled glomerular annotations from the childhood-onset lupus nephritis spatial dataset. The analyzed layer contained 532,392 segmented cells across 279 fields of view from 14 tissue samples: 10 LN tissue samples from 8 SLE/LN patients and 4 control samples. Disease classes in the LN tissue samples were class III (4 samples), class IV (5 samples), and class IV+V (1 sample). Cell classes were taken from the cleaned object and collapsed into broad groups including myeloid, glomerular, tubular, endothelial, stromal, B/plasmablast, and T/NK. The analysis retained 11,805 myeloid cells.

Glomerular regions were defined from the bundled polygon annotations. The analysis included 620 glomerular polygons, with 264 in LN tissue samples and 356 in controls. Each segmented cell was assigned to inside-glomerulus, glomerular-border, or tubulointerstitial context and to a glomerulus-centered distance ring using the nearest glomerular centroid and equivalent-radius-normalized distance. Myeloid fraction was calculated as myeloid cells divided by all segmented cells within each sample-level

spatial context or distance bin; distance profiles were summarized at the sample level. Equivalent radius was the square root of polygon area divided by pi. Normalized distance bins were [0, 0.5), [0.5, 1), [1, 1.5), [1.5, 2), [2, 3), and [3, infinity).

CosMx spatial module scores were calculated as mean log2(CPM + 1) over measured genes only, with absent genes not imputed. For the manuscript IFN module, the component used 7 measured genes of 21 (*IFI27, IFIT1, LAMP3, MX1, OAS1, OAS2, OAS3*). *PLAUR* was not measured in this CosMx panel.

Treatment response

For the AMP dataset, patient treatment response labels were binned into two groups, "Non-Responders" for patients without response and "Responders" for patients with partial or complete response. Patients with "Other" or "Missing" labels were excluded. Cell fractions were plotted as above. The baseline comparison included 43 responders (26 complete and 17 partial) and 48 nonresponders with evaluable scores. Plots are labeled with the p-value from results of two-sided Wilcoxon rank-sum tests. BH correction was applied separately across score/compartment tests within the response contrast.

Human samples for genotyping

Data from 131 active lupus cases consisting of patients of self-reported European ancestry that had serum available for suPAR analysis were obtained from Rush University Medical Center and Mayo Clinic (18). Informed consent was obtained from all patients in all the cohorts included in this study, and the study was approved by the Institutional review boards at the respective institutions.

Genotyping

Patients were genotyped as described previously (19). Briefly, genotyping at coding change SNPs in *ITGAM* (rs1143678, rs1143679 and rs1143683) was performed using custom designed Applied Biosystems Taqman primers and probes on an Applied Biosystems 7900HT PCR machine with >98%

genotyping success. Genotyping scatter plots were all reviewed individually for quality, and genotype frequencies did not deviate significantly from the expected Hardy-Weinberg proportions ($p>0.01$).

Human PBMC isolation

Human peripheral blood mononuclear cells (PBMCs) were isolated from fresh blood collected from healthy volunteers under an IRB-approved protocol and using RosetteSep (human monocyte Enrichment Cocktail, Cat# 15068 Stemcell Technologies, Vancouver, Canada) followed by Ficoll-Hypaque density gradient centrifugation according to published protocols(20). Briefly, blood was diluted with PBS containing 2% FBS and was layered on the top of the ficoll-paque solution very gently. The tubes were centrifuged at 400g for 20 minutes at room temperature using slow acceleration and deceleration, and the upper plasma layer was removed carefully. The buffy coat (PBMCs) from plasma-ficoll interphase was transferred to a clean tube and DPBS was added and mixed well. Again, it was spun at 100g for 10 minutes to remove any contaminating Ficoll and platelets/proteins. The cells were washed with DPBS, resuspended in RPMI-1640 with GlutaMAX (Cat# 61870-036, GIBCO), supplemented with 10% FBS and seeded into T75 (75 cm2) tissue culture flask (Cat#156800, Thermo). Non-adherent cells were removed by gentle pipette aspiration after 2h of incubation at 37°C in a humidified atmosphere containing 5% CO_2. Subsequently, an equal volume of fresh complete medium was added to each flask and the cells were placed back in the incubator for approx. 24h (21, 22).

Cell line

The cell line RAW 264.7 murine macrophage was obtained from the American Type Culture Collection (ATCC #TIB-71) and was maintained accordingly.

Mice

The C57BL/6J (B6) wild type (cat# 000664) (CD11b WT), B6 CD11b$^{-/-}$ (cat# 003991) (23) (CD11b KO), female MRL/lpr (cat# 000485) and haplotype-, age- and sex-matched control MRL/MpJ

(cat# 000486) were from The Jackson Laboratory, Bar Harbor, ME. To examine role of genetic activation of CD11b on TLR7-dependent lupus nephritis, we used transgenic mice that we recently generated expressing a constitutively activated CD11b by introducing an I332G point mutation in the murine Itgam gene (C57BL/6 *ITGAM*^{I332G})(24) (CD11b KI). The mice were maintained in specific-pathogen-free conditions and used in accordance with the Institutional Animal Care and Use Committee (IACUC) and the respective institutional guidelines. The MRL/MpJ mice were used as a non-lupus prone, haplotype-matched strain to compare lupus-prone mice to normal pathology. Our study mostly examined female mice because SLE has a 9:1 prevalence in females.

TLR7-induced mouse model

8-10 weeks old C57BL/6J wild-type, CD11b$^{-/-}$ or CD11b KI female mice were treated with imiquimod (IMQ) according to published protocols to induce TLR7-induced systemic lupus (25). Briefly, the skin on the right ears of the mice were treated topically with 1.25 mg of 5% imiquimod cream three times per week for 8-10 weeks. The ultraviolet B (UVB) irradiation was also applied for 30s using Dermaray M-DMR-1 lamp bulbs with peak emission at 311 nm. For the treatment groups, mice were treated with ONT01 (30mg/kg BID) or vehicle (1% Tween-20 in sterile saline) orally twice daily. Treatment began concurrently with IMQ in the preventive experiment and 2 or 4 weeks after IMQ induction in the delayed-treatment experiments. Urine was collected every other week. At the end of the experiment, blood was collected by terminal cardiac puncture and processed for sera and PBMCs. Ears and kidneys were harvested for RNA, protein, and histology. Macrophages were generated from bone-marrow derived monocytes and cultured in RPMI containing 10% FBS cultured for 5-7 days. Spleen was isolated for measurement of size and weight and for flow cytometric analyses. For the preventive IMQ experiments shown in Fig. 4F,H,J and Fig. S15a-c,e, IMQ-alone and IMQ-plus-vehicle observations were pooled into a single disease-control group, retaining all individual observations.

MRL/lpr mouse model

8-week old mice were obtained from the Jackson Laboratory (Bar Harbor, ME). Female MRL/lpr mice were treated orally with ONT01 (30mg/kg) or vehicle (1% Tween-20 in sterile saline) twice daily, beginning at 8 weeks of age in the early-treatment experiment or at 10 weeks in the delayed-treatment experiment, and continuing until euthanasia at 20 weeks of age (26). Haplotype-matched female MRL/MpJ mice were used as phenotypic controls. Kidneys and affected skin samples were harvested after perfusion with PBS (Phosphate Buffered Saline). Regions of alopecia were measured on the face and dorsum, with greatest diameter determined to the nearest millimeter with calipers. Paraffin embedded sections (4 μm) were stained with hemotoxylin-eosin (H&E) or periodic acid-Schiff (PAS). The assessments were blinded for histological analysis. Sample size was chosen based on previous studies using interventions in MRL/*lpr* mice to assess similar outcomes in phenotype (18).

Humanized mouse model

Wild-type female C57BL/6J mice or NOD-scidIL2γnull NSG mice were purchased from the Jackson Laboratories. 6–8 weeks old mice were housed under pathogen-free conditions in the animal facility at the Rush University Medical Center in accordance with the institutional guidelines under Institutional Animal Care and Use Committee approval. Human LN patient blood was used and isolated PBMCs were injected intravenously (*i.v.*) into NSG mice (2.5 x 10^6 cells per mouse) on day 0. For the treatment groups, mice were treated with ONT01 (30mg/kg) or vehicle (1% Tween-20 in sterile saline) orally once daily, starting at 2 weeks post engraftment. R77H mice were treated with LA1 (6mg/kg) or vehicle intraperitoneally (*i.p.*) twice daily, starting at 2 weeks post engraftment. The humanized mice were monitored daily for overt clinical signs (alopecia, skin lesions, weight loss & arthritis), morbidity and mortality. Body weights were recorded weekly and skin lesions were photographed and scored weekly.

Whole blood sampling for serum and FACS analysis of human cell engraftment rates

A small sample of peripheral blood was drawn from the mice under general anesthesia 2-, 4- and 6-weeks post-humanization by penetrating the retro-orbital sinus in mice with a glass capillary tube. The blood sample was split for FACs analysis and serum preparation. For FACs staining, an anticoagulant was added to the blood, RBCs were lysed, and the isolated leukocytes were stained with fluorescence-labeled antibodies against human CD45 and mouse CD45 for flow cytometry-based quantification to confirm high human cell engraftment rates. For serum, the whole blood was clotted at room temperature for 30 minutes, followed by a 10-minute centrifugation at 2,000g. The RBC free serum was transferred into micro-centrifuge tubes and stored at -80° C until further analysis.

Mouse model of severe sepsis

To induce experimental sepsis, we utilized our previously published model (Colaço et al., Immunity, 2020). Briefly, mice (female C57Bl6/J, 11 weeks) were injected intraperitoneally with 200 µL of a bacterial suspension containing 5×10^8 E. coli K12 MG1655 (Strep resistant). Mice were treated with ONT01 (30mg/kg) or vehicle (0.5% methylcellulose and 0.02% Tween 80) orally at 0 and 8h post-infection. Vital parameters were collected over 5 days or animals were sacrificed at 24h for sample collection (blood via cardiac puncture, organs, and peritoneal lavage fluid). Bacterial load in organs and fluids was assessed by plating serial dilutions on LB + Strep agar plates.

Preparation of murine bone marrow derived macrophages

Mice were euthanized via CO2 and secondary cervical dislocation, and the bone marrow cells from tibia and femurs were collected by flushing with DMEM containing 10% FBS and using a 25-gauge needle according to published protocols (18). Any cell clumps were dispersed by gently pipetting the solution and then passed through a 70µm cell strainer. The suspension was subsequently centrifuged, the supernatant discarded, and the pelleted cells gently resuspended in DMEM containing 10% FBS. Red blood cells were removed by treating the cell suspension with RBC lysis buffer according to manufacturer's instructions. Cells were washed and resuspended in DMEM containing 10% FBS. For

generation of bone marrow derived macrophages, approx. 8 X 10^6 cells were seeded in 6 mL of DMEM containing 10% FBS and 50 ng/mL MCSF (PeproTech #315-02) in a 100mm plate on day 0. Cells were cultured for 7 days and fed with an additional 3mL media with 50ng/mL MCSF on day 4 of culture. On day 7, cells were removed from the plates with an EDTA solution, viability was checked, and cells were re-plated using DMEM with 1% FBS before planned treatments.

NF-κB and STING Agonist treatment

CD11b KI BMDMs were treated with NF-κB agonist (Phorbol myristate acetate, PMA) at 200 ng/mL and STING agonist (ADU-S100) at 1μg/mL for 4 hours. Cell supernatant was used in ELISA experiments.

Analysis of albuminuria

Mouse urine samples were collected, transferred into a microcentrifuge tube and stored at -80° for future analysis. Urinary albumin concentration was measured using a mouse albumin ELISA (Bethyl Laboratories, Montgomery, TX #E99-134) and urinary creatinine assay (Exocell, Philadelphia, PA #1012), respectively, according to manufacturer's protocol. Subsequently, urine albumin:creatinine (ACR) ratio was calculated.

Quantification of suPAR, and anti-dsDNA Antibody

Mice sera and RAW cell supernatants were used for quantification. Commercial ELISA kits for murine anti-dsDNA antibodies (Alpha Diagnostic #5120), and suPAR (R & D system #DY531) were performed according to the manufacturer's instruction.

ELISA assays for cytokine readout

Cell supernatants and blood were collected for cytokine analysis by ELISA and were prepared by centrifugation and isolation of supernatant that was frozen until use. Cytokine levels (IFN-b, IL-6, TNF-a)

were measured by ELISAs ordered from R&D Systems and were performed according to manufacturer's protocol. Briefly, mouse macrophages were cultured in the presence of vehicle (1% DMSO), ONT01 (20 μM), IMQ (20μg/mL), or IMQ + ONT01 for 6 h and the cell supernatant was collected. Mouse cell culture supernatants were assayed using commercially available sandwich ELISA kits for mouse IL6 (R&D Systems, Minneapolis, MN, catalog# M6000B), and TNF-α (R&D Systems, Minneapolis, MN, catalog# MTA00B) according to manufacturer's instruction. For measuring IFN-β levels, mouse macrophages (WT and CD11b$^{-/-}$ and KI) were cultured in the presence of vehicle (1% DMSO), ONT01 (20 μM), IMQ (20μg/mL), or IMQ + ONT01 for 12h and the cell culture supernatant were assayed using commercially available sandwich ELISA kits for mouse IFN-β (PBL Assay Science, Piscataway, NJ, catalog# 42400-1) according to manufacturer provided instructions.

Histology

One part of the removed kidney was fixed in 10% formalin and embedded in paraffin and another part was immediately snap frozen in OCT on liquid nitrogen and stored at -80°C. Samples were labelled and sent to the University of Illinois at Chicago Research Histology Core for sectioning and staining. Paraffin embedded sections (4 μm) were stained with hemotoxylin-eosin (H&E) or periodic acid-schiff (PAS). Stained slides were blindly evaluated by an experienced pathologist for chronic tubulointerstitial damage, glomerular sclerosis, and tubulointerstitial inflammation using 0 (none), 1+ (<25%), 2+ (25-50%), 3+ (>50%) scoring system. Formalin-fixed and frozen sections of the skin were prepared as for kidneys.

Immunohistochemistry and Immunofluorescence

For immunofluorescence studies, tissue sections (4 μm) were cut and fixed in -20°C acetone before immunofluorescence staining. Sections were blocked (4% FBS, 4% BSA, 0.4% Fish gelatin in PBS) at room temperature for 1 hr and incubated with the appropriate primary antibodies in blocking buffer at 4°C overnight. Sections were incubated with the appropriate secondary antibody (Thermofisher

Scientific) and mounted with DAPI medium (Vector Laboratories). Fluorescence images were acquired using a Zeiss LSM 700 confocal microscope with a PLAN-Apochromat 20 X objective and an AxioCam camera and analyzed using the Zen software (Carl Zeiss Group). The number of WT1 positive cells per glomeruli was calculated manually using the confocal microscope (5 glomeruli/tissue). The fluorescence intensities for synaptopodin, C3, 9EG7, IgG, CD11b and F4/80 were calculated using the ImageJ Software (5-8 glomeruli/tissue).

Flow cytometry of mouse splenocytes and kidney tissues for immunophenotyping

Single cell suspensions of mouse splenocytes were prepared using a cell strainer, rinsing with FACS buffer. The cells were washed with PBS and then underwent RBC lysis using 1x multi-species RBC Lysis Buffer (Cat#00-4333-57, eBioscience). The cells were washed again in PBS and resuspended in FACS buffer (2% FBS in PBS) at 1.0 x 10^6 cells/mL for analysis by flow cytometry. After blocking for 15 minutes, cells were resuspended in 100uL FACS buffer and incubated with 2uL each of respective antibodies or isotype control for 30 minutes/ 1 hour on ice, fixed with BD stabilizing fixative, quantified by flow cytometry using LSR Fortessa research only use (ROU) or BD FACSCanto RUO and data analyzed using FlowJo software (FlowJo LLC, Ashland, OR). Cutoff values for positive staining were determined using compensation controls for each fluorophore. Results were reported as number of cell subsets/million splenocytes.

Single cell suspensions of mouse kidney were prepared with RPMI with 10mg/mL collagenase IV (Sigma Cat# 5134) and 10mg/mL DNase I (Roche Cat# 1 0104159 001). Approximately 1.0 x 10^6 cells/mL were taken for analysis by flow cytometry. The cells were washed and resuspended in 1 mL of PBS and 1 uL of Live/Dead Fixable Aqua was added to the samples. After, 30 minutes of incubation at room temperature in the dark. The cells were washed and resuspended in 200 uL FACS buffer (0.5% BSA in PBS) and incubated with respective antibodies for 30 minutes at 4°C in dark. The cells were washed and resuspended in 100 uL 4% PFA, left in dark at 4°C, overnight. The cells were washed in PBS next day, resuspended in 250 uL of FACS buffer and filtered using 40 μm filters, before quantification by

flow cytometry using LSR Fortessa research only use (ROU) and data analyzed using FlowJo software (FlowJo LLC, Ashland, OR). Cutoff values for positive staining were determined using compensation controls for each fluorophore. Results were reported as number of cell subsets/million kidney cells.

Transmigration Assay

The human monocytic THP-1 cells (ATCC, TIB-202) were pre-treated with ONT01 (20 μM) or vehicle control for 30 min prior to seeding (5×10^5 cells per well) in the upper chambers of a 24-well transwell plate (Corning, 8 μm). The bottom chambers were filled with media alone or media containing CCL2 (50 ng/mL). THP-1 monocytes that transmigrated to the bottom wells after 6 h were collected and counted using an automated cell counter (ViCellXR). Percent migration was calculated as: (cells migrated in the bottom chamber)/(total cells seeded in the upper chamber) × 100 and reported.

Quantification of inflammatory markers by qPCR

RAW 264.7 cells in culture were washed with PBS and lysed using 700μL of Trizol. Kidney tissues were homogenised in Trizol followed by RNA extraction using RNeasy Mini kit (catalog #74106, Qiagen) according to manufacturer's protocol. cDNA was synthesized using iScript Reverse Transcription Supermix (cat #1708841, BioRad) according to manufacturer's instruction. cDNA, desired primers, and SsoAdvanced Universal SYBR Green Supermix (cat #1725271, BioRad) were subjected to quantitative Real-time PCR using thermal cycler according to the manufacturer's instruction and relative changes in gene expression were analyzed using the formula $2^{-\Delta\Delta Ct}$. All inflammatory marker genes including housekeeping gene (PPIA/GAPDH) were quantified. The primer sequences for the uPAR, IFNβ, IL6, and TNFα genes have been described by our group previously (18). Primer sequence are as follows: mouse *CCL2* forward primer 5'-GTCCCTGTCATGCTTCTGG-3', mouse *CCL2* reverse primer 5'- TCTTGCTGGTGAATGAGTAGC-3'; mouse *PPIA* forward primer 5'-CAAACACAAACGGTTCCCAG-3', mouse *PPIA* reverse primer 5'- TTCACCTTCCCAAAGACCAC-

3’; mouse *GAPDH* forward primer 5’- CCTCGTCCCGTAGACAAAATG-3’, mouse *GAPDH* reverse primer 5’- CAATCTCCACTTTGCCACTG-3’.

Western Blot

Cells were lysed with RIPA buffer containing EDTA (Cat #BP-115D, Boston Bioproducts) and cocktails of protease inhibitor (Catalog #11836170001, Millipore Sigma) and phosphatase inhibitor (cat #PI78420, Thermo Fisher Scientific). Protein concentration was calculated with the Pierce BCA Protein Assay Kit (Cat #23227, Thermo Fisher Scientific) according to manufacturer’s protocol and the samples were aliquoted accordingly before freezing for future use. Samples were thawed on ice. NuPAGE LDS Sample Buffer (catalog #NP0007, Invitrogen) with 1% β-mercaptoethanol was added to each sample before denaturing them at 90°C for 5 minutes. Equal amounts of proteins were loaded in wells of a 4-12% NuPAGE Bis-Tris Gel (cat #NP0322BOX, Invitrogen) and blotted to a PVDF membrane (catalog #IPFL00010, EMD Millipore). Subsequently, the membrane was blocked with blocking buffer (5% BSA in PBS) for 1 hour at RT followed by incubation with primary antibodies in assay buffer (0.5% BSA and 0.05% Tween-20 in PBS) overnight at 4°C. Subsequently, the membranes were washed with assay buffer and incubated with anti-rabbit or anti-mouse secondary antibody in assay buffer for 1 hour at RT. Proteins were detected using either a LI-COR odyssey imager or incubation with Pierce ECL western blotting substrate and imaged with X-ray film. Data presented is representative of at least three independent experiments.

Human Macrophage Perturbation Re-analysis

For the human macrophage perturbation analysis, we used the public GEO accession GSE76802 (18), originally generated from primary human monocyte-derived macrophages treated with DMSO, LA1, LPS, or LPS+LA1 under the protocol deposited with the accession. Duplicate probe rows were collapsed to one record per gene by selecting the probe with the highest grand mean expression across all 12 samples, yielding 31,332 unique gene-level records. Differential expression was performed with limma

(27) using a paired design for LPS versus DMSO, LPS+LA1 versus LPS, and LA1 versus DMSO. Canonical IFN and Hallmark TNFA/NF-kB gene sets were evaluated using DMSO-centered per-gene z-score sample scores, limma camera competitive gene-set tests, limma fry pathway summaries, and direction-aligned gene-level effect summaries.

Human Pharmacokinetic Profile Analysis

Plasma concentration-time data from the GB1275 (ONT01) first-in-human trial (ClinicalTrials.gov ID: NCT04060342) were linked to cohort annotations by normalized subject identifiers. Concentrations reported as <1.00 ng/mL were set to 0 for linear-scale visualization. Day 1 observations from 0 to 24 hours after dosing were retained for subjects receiving 100, 200, 400, or 800 mg BID using the 100 mg tablet formulation. Samples were grouped by nominal post-dose time and planned dose, and arithmetic mean plasma concentration with standard error of the mean (SEM) was calculated at each time point. Profiles were plotted descriptively on the linear concentration scale in ng/mL.

OLink Response Analysis for Human Clinical Trial Data

OLink proteomic data from the GB1275 (ONT01) first-in-human trial (ClinicalTrials.gov ID: NCT04060342) was linked to cohort and visit annotations by normalized subject identifiers. Briefly, blood samples were taken pre-dose and 2 hours post dose at each visit. OLink NPX units were treated as log2-scale relative protein levels per plate barcode. NPX values were adjusted within each protein by centering plate-specific reference means to the study-wide protein reference mean. Baseline was anchored to Day 0 pre-dose measurements. For volcano plots, Day 0 baseline and Day 15 on-treatment trough observations were collapsed to subject-level means for each protein, regimen, and time point. Regimen A and Regimen B were analyzed separately. For each protein within each regimen, paired protein movement was calculated as Day 15 minus Day 0 plate-adjusted NPX on the log2 scale. Volcano plots display the mean paired Day 15-Day 0 log2 NPX change on the x-axis and the corresponding -log10 paired-test P

value on the y-axis. Positive values indicate higher protein abundance at Day 15 relative to Day 0, whereas negative values indicate lower abundance at Day 15. P values were adjusted across proteins within each regimen using the Benjamini-Hochberg procedure.

Statistics

The general statistical approach is stated in the Statistics section of the main-text Methods. The AMP single-cell analyses are specified here.

For AMP human data, donor-level comparisons were used for statistical testing so that cells from the same donor were not treated as independent observations. Unpaired two-group comparisons used two-sided Wilcoxon rank-sum tests. Multi-group Canonical IFN comparisons used Kruskal-Wallis tests with Wilcoxon rank-sum tests for pairwise group comparisons. Pseudobulk differential expression used donor-level count aggregation followed by edgeR normalization (28) and limma-voom modeling, with ancestry PC adjustment for genotype contrasts when applicable. Multiple-testing correction used the Benjamini-Hochberg method within the relevant family of tests. Box plots show median and interquartile range with individual donor values overlaid unless otherwise specified.

For the AMP carrier-versus-noncarrier comparison, the canonical IFN21 gene set was evaluated using the limma CAMERA competitive gene-set test (27), which accounts for inter-gene correlation and compares the signature with the tested transcriptomic background. The count-based CAMERA analysis (limma 3.62.2) used 120 LN donors, at least 30 myeloid cells and complete PC1-PC5. Full-RNA donor count sums were filtered with edgeR filterByExpr, TMM-normalized and analyzed with voom using ~ genotype + PC1 + PC2 + PC3 + PC4 + PC5 (carrier minus non-carrier). The tested universe comprised 21 IFN21 and 10,430 background genes. camera P value was nominal for one primary competitive hypothesis. Gene-wise BH correction covered all 10,451 tested genes.

Within LN, the association between R77H carrier status and the donor-level kidney myeloid canonical IFN score was evaluated with adjustment for age, sex, ancestry principal components, myeloid

cell number and myeloid-subset composition. Adjustment for the regulatory marker rs3087796 was evaluated separately. The LN-versus-control IFN-score comparison also used donor-level covariate and composition adjustment. Adjusted differences were reported with 95% confidence intervals and nominal P values. For the original-genotype kidney-myeloid model, the outcome was the unitless IFN21 score and covariates were age per decade, sex, PC1-PC3, log10 myeloid cell count and within-myeloid monocyte, granulocyte and dendritic/mast-cell fractions, with macrophages as reference. The adjustment stages used the same 127 complete-case LN donors (32 carriers/95 non-carriers); the composition-adjusted coefficient was 0.300 (95% CI 0.015-0.585). The LN-versus-control model used the same covariate structure in 150 LN and 24 control complete cases after excluding five donors from each group because of insufficient myeloid cells or unavailable genotype data. Separate rs3087796 models used the genotype and PC1-PC5, with identical complete cases within each comparison (kidney n = 127; blood n = 99). These linear models used HC3 standard errors and residual-degrees-of-freedom t tests and 95% confidence intervals.

Supplementary Figures

ITGAM variants do not alter blood-cell counts

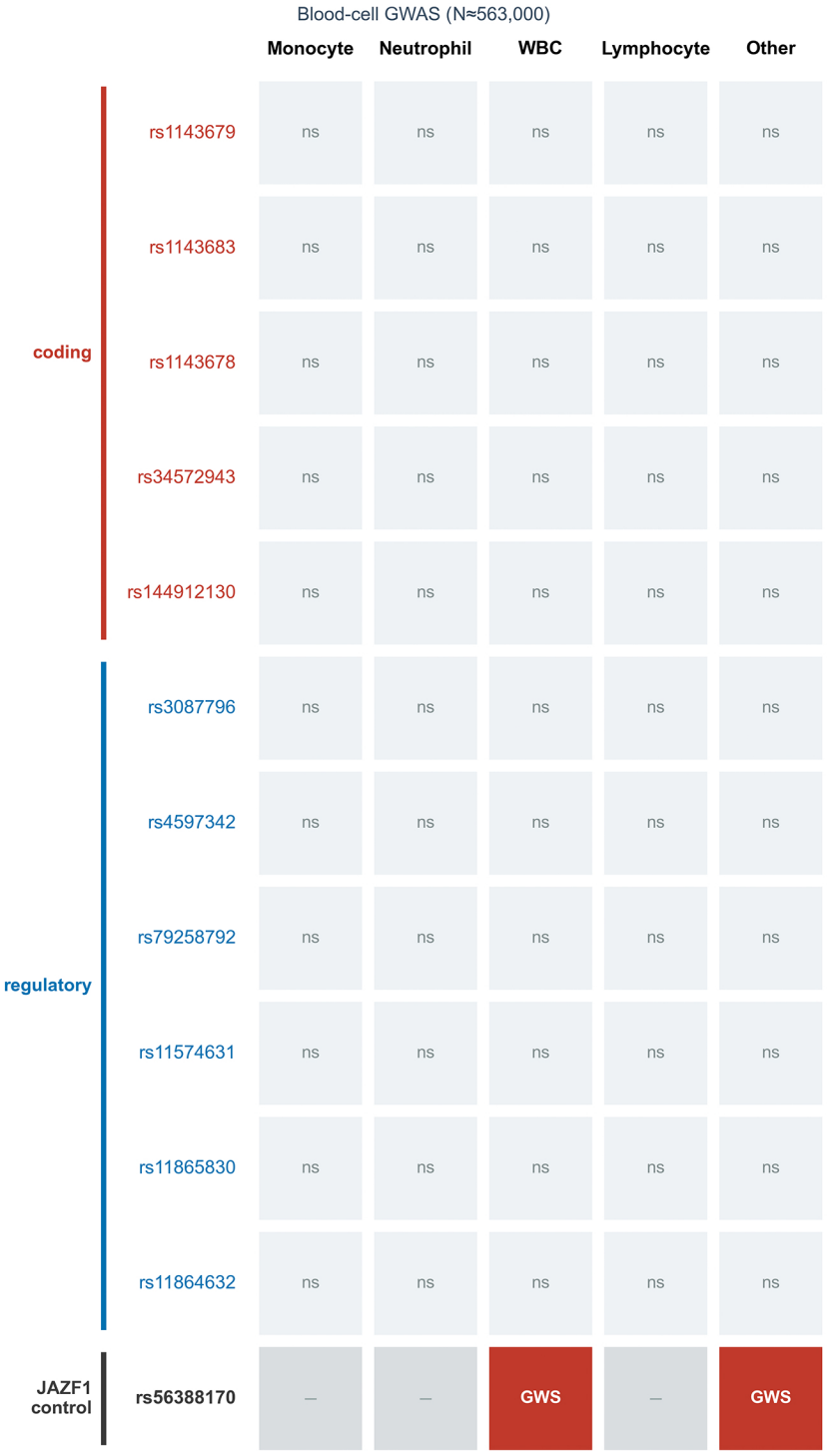

Figure S1

Figure S1. No detected genome-wide significant associations between ITGAM haplotype variants and blood-cell counts. Matrix summarizing curated blood-cell GWAS evidence for five variants in the R77H-linked coding haplotype and six variants in the regulatory haplotype across monocyte, neutrophil, total white-blood-cell, lymphocyte, and other blood-cell traits. Each cell indicates whether the variant reached genome-wide significance in the blood-cell GWAS datasets used in the analysis, with a combined sample size of approximately 563,000 individuals. Data were derived from the GWAS Catalog, dbSNP, and the blood-cell GWAS studies (29–31). ns, no genome-wide significant association; GWS, genome-wide significant association; –, not reported. The JAZF1 variant rs56388170 is shown as a positive control.

ITGAM R77H raises coherent IFN program in plasma

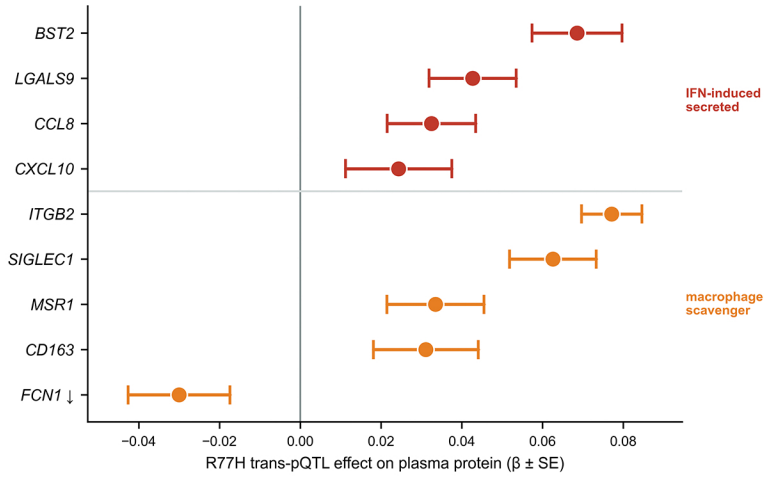

Figure S2

Figure S2. *ITGAM* R77H raises a coherent interferon–myeloid protein program in plasma. Forest plot showing per-allele trans-pQTL effect estimates for rs1143679 across nine plasma proteins identified in the plasma proteomic analyses (5, 10). Points show effect estimates and error bars show standard errors. Red denotes IFN-associated secreted proteins, including BST2, LGALS9, CCL8, and CXCL10. Orange denotes ITGB2 and myeloid activation- or scavenger-associated proteins, including SIGLEC1, MSR1, CD163, and FCN1. The vertical line indicates the null effect. FCN1 is the only protein with a negative estimated effect.

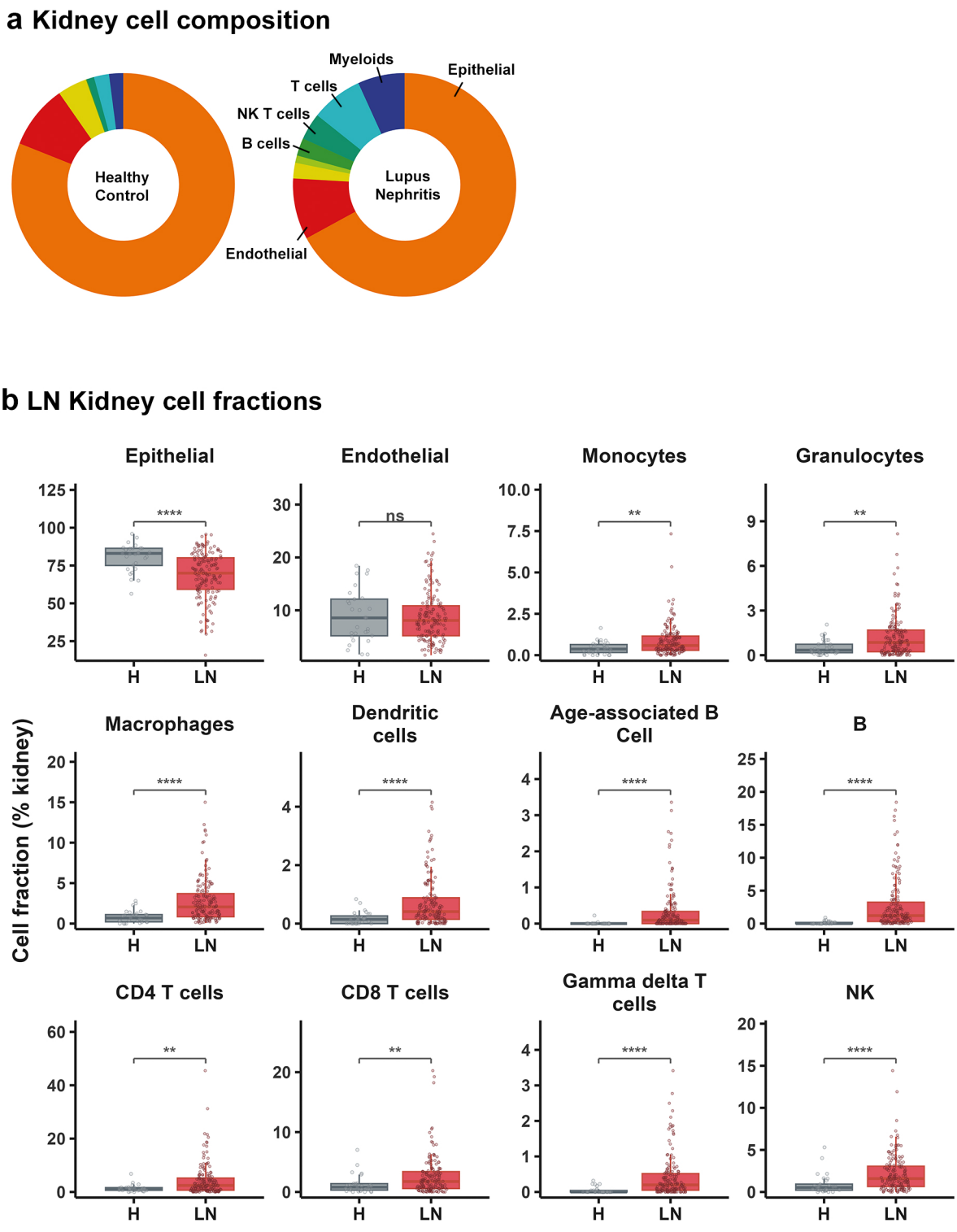
a Kidney cell composition
Healthy Control
Lupus Nephritis
Myeloids
Epithelial
T cells
NK T cells
B cells
Endothelial
b LN Kidney cell fractions
Epithelial
Endothelial
Monocytes
Granulocytes
Macrophages
Dendritic cells
Age-associated B Cell
B
CD4 T cells
CD8 T cells
Gamma delta T cells
NK
Cell fraction (% kidney)
H
LN
****
ns
**

Figure S3

Figure S3. CD11b+ myeloid and other immune cells are enriched in LN patient kidneys. a. Aggregate proportions of major epithelial, endothelial, and immune-cell populations in healthy-control and lupus nephritis (LN) kidney samples. **b.** Donor-level kidney fractions of epithelial cells, endothelial cells, monocytes, granulocytes, macrophages, dendritic cells, age-associated B cells, B cells, $CD4^+$ T cells, $CD8^+$ T cells, γδ T cells, and natural killer cells in healthy controls (H; n = 29) and patients with LN (n = 155). Points represent donors, and boxplots show the median and interquartile range. Comparisons were performed using Wilcoxon rank-sum tests. ns, not significant; Two, three, and four asterisks denote $P < 0.01$, $P < 0.001$, and $P < 0.0001$, respectively.

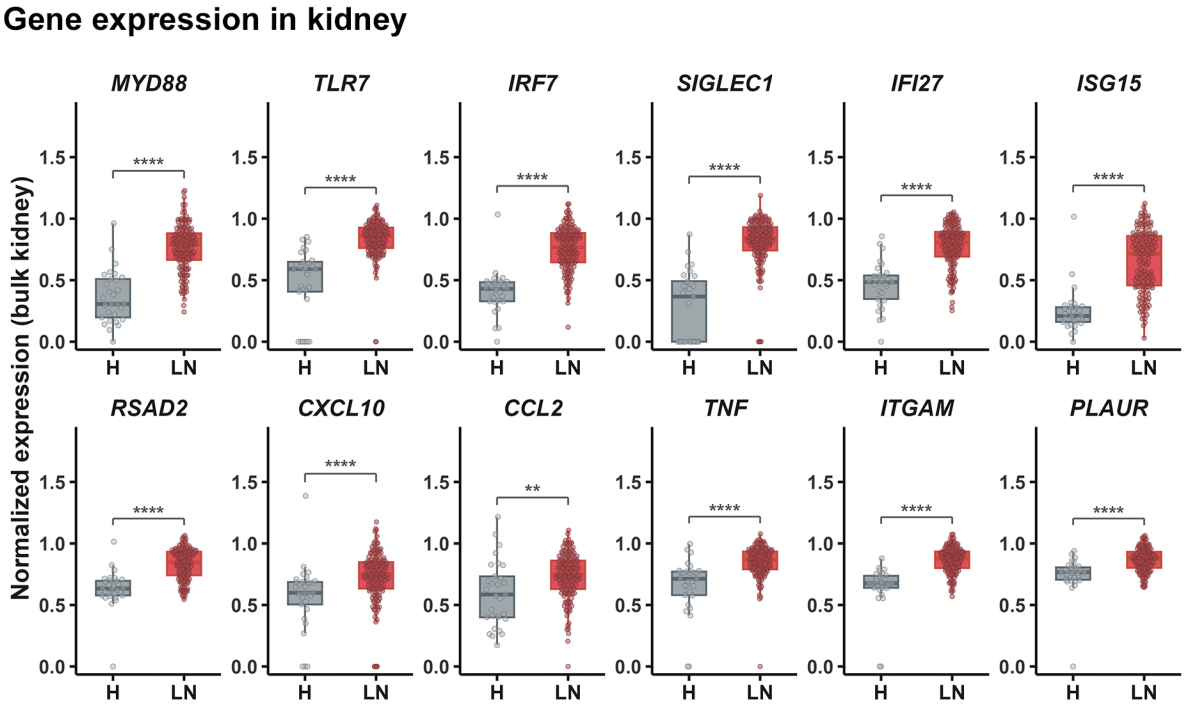
Gene expression in kidney
MYD88
TLR7
IRF7
SIGLEC1
IFI27
ISG15
RSAD2
CXCL10
CCL2
TNF
ITGAM
PLAUR
Normalized expression (bulk kidney)
H
LN
****
**
0.0
0.5
1.0
1.5

Figure S4

Figure S4. Inflammatory gene expression is increased in LN patient kidneys. Normalized bulk-kidney expression of MYD88, TLR7, IRF7, SIGLEC1, IFI27, ISG15, RSAD2, CXCL10, CCL2, TNF, ITGAM, and PLAUR in healthy controls (H; n = 29) and patients with lupus nephritis (LN; n = 155). Points represent donors, and boxplots show the median and interquartile range. comparisons were performed using Wilcoxon rank-sum tests. Two, three, and four asterisks denote $P < 0.01$, $P < 0.001$, and $P < 0.0001$, respectively.

Spatial organization of IFN-I–high myeloid cells in LN glomeruli

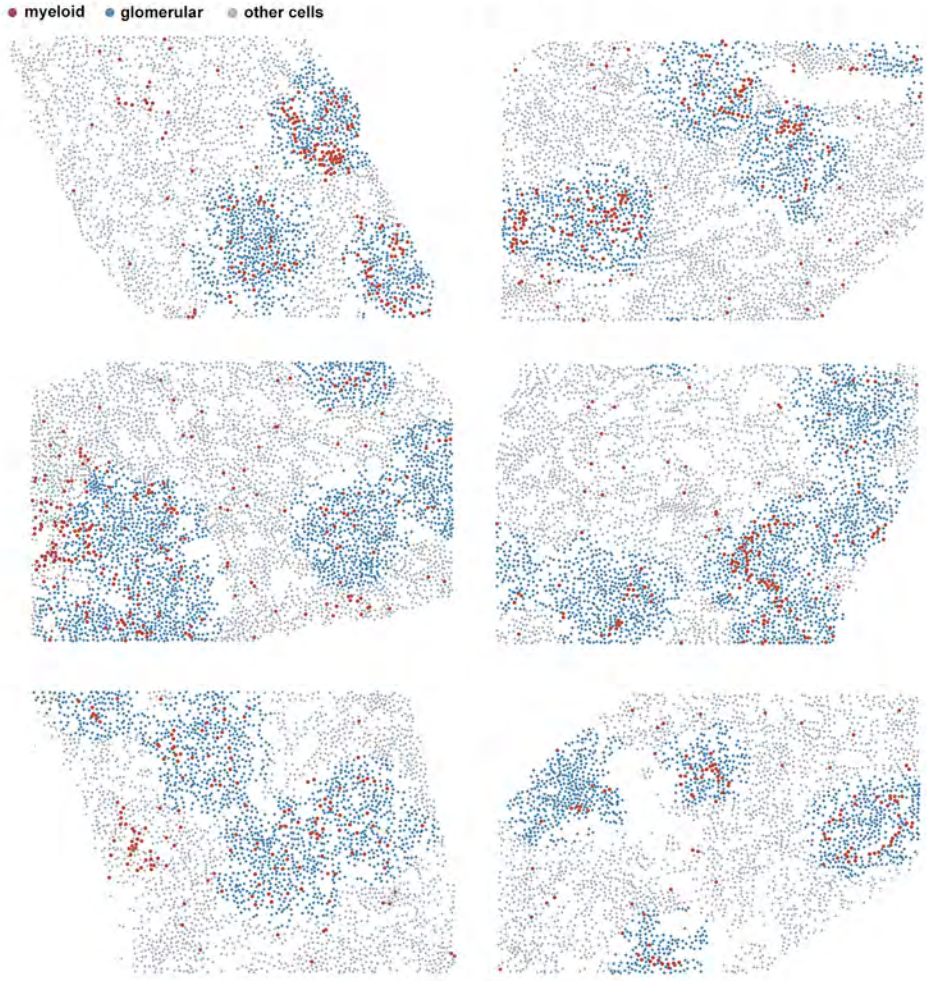

Figure S5

Figure S5. IFN-I–high myeloid cells colocalize with LN glomeruli. Representative CosMx field of view in multiple LN tissue samples from the independent childhood-onset LN CosMx cohort showing myeloid cells, glomerular cells, and other cells, as labeled.

Molecular model of CD11b bound to ONT01

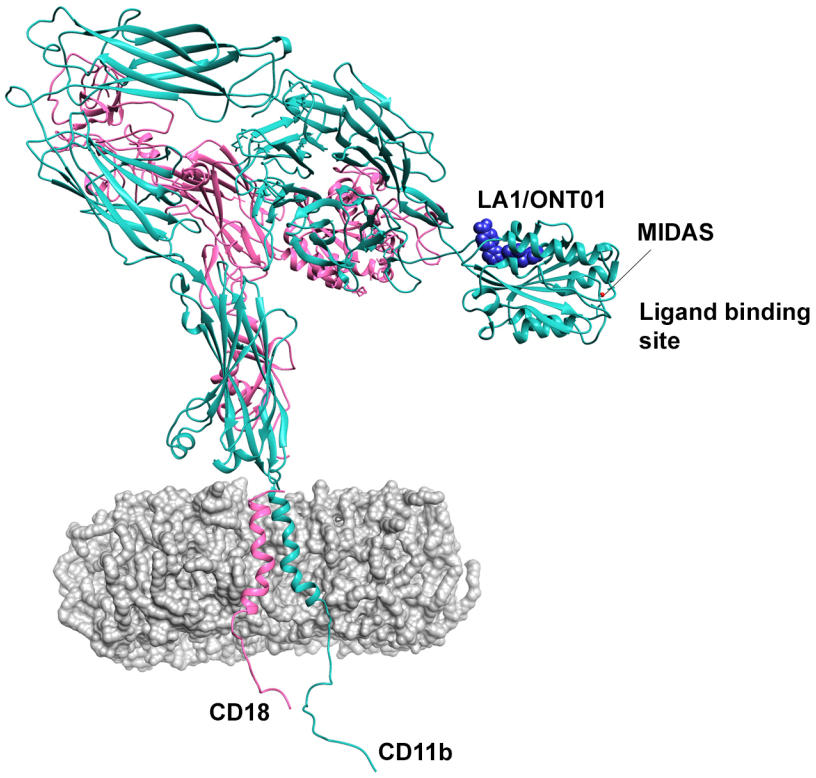

Figure S6

Figure S6. Molecular model of the CD11b/CD18 integrin with the small-molecule agonist LA1. Structural model of the CD11b/CD18 heterodimer based on the published αXβ2 integrin structure. CD11b is shown in cyan, CD18 in pink, and the plasma membrane in gray. LA1/ONT01, the small-molecule CD11b agonist, is shown in the activation-sensitive allosteric pocket near the F–α7 region of the CD11b αA/I domain (ONT01 is a choline salt of LA1). The ligand-binding site and the metal ion at the metal-ion-dependent adhesion site (MIDAS) are indicated.

a. RAW Cells

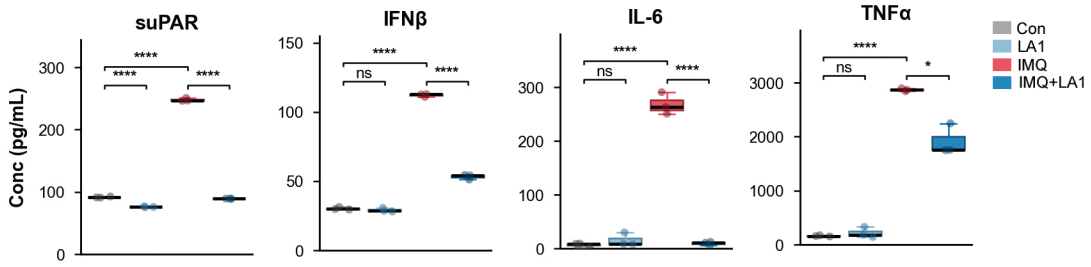

b. RAW cell qPCR

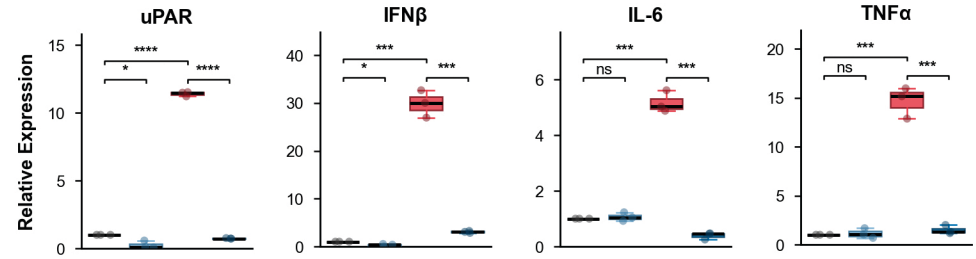

c. NF-kB Treatment

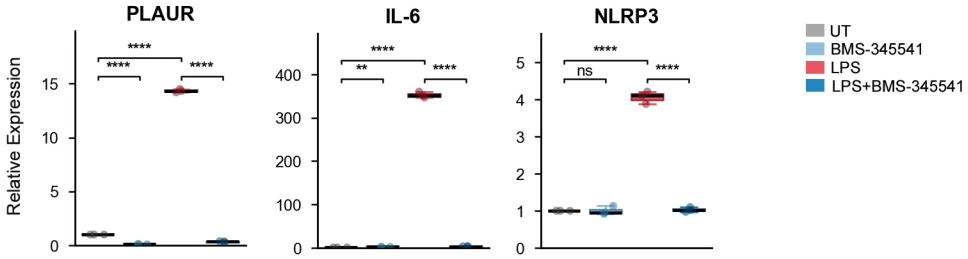

Figure S7

Figure S7. Pharmacologic CD11b activation and IKK inhibition suppress TLR-induced inflammatory outputs in RAW264.7 macrophages. a. ELISA-based quantification of suPAR, IFNβ, IL-6, and TNFα in supernatants from untreated cells (UT), cells treated with LA1 alone (20 μM), cells stimulated with imiquimod (IMQ) (20 μg/ml), or cells stimulated with IMQ in the presence of LA1. **b.** Relative expression of uPAR, IFNβ, IL-6, and TNFα transcripts under the same treatment conditions. **c.** Relative expression of PLAUR, IL6, and NLRP3 in untreated cells, cells treated with the IKK inhibitor BMS-345541 [1 μM], cells stimulated with LPS (50 ng/ml), or cells stimulated with LPS in the presence of BMS-345541. Data show mean ± s.e.m. (n = 3). ns, not significant; one, three, and four asterisks denote $P < 0.05$, $P < 0.001$, and $P < 0.0001$, respectively. Comparisons between two groups used two-tailed unpaired t-tests with Welch's correction and among three or more groups used one-way ANOVA with Tukey's multiple-comparison test.

a. Pharmacologic and genetic activation of CD11b suppresses TLR4-induced *Plaur*/suPAR in BMDMs

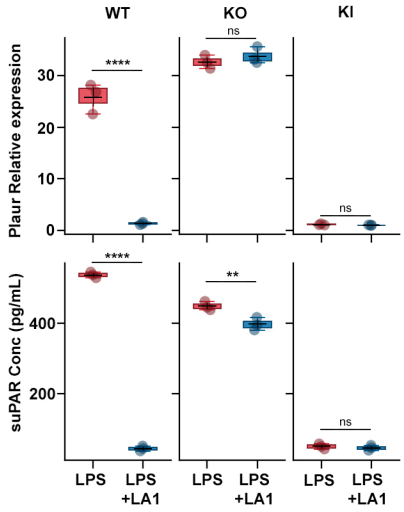

b. Pharmacologic and genetic activation of CD11b suppresses TLR7-induced inflammatory markers in BMDMs

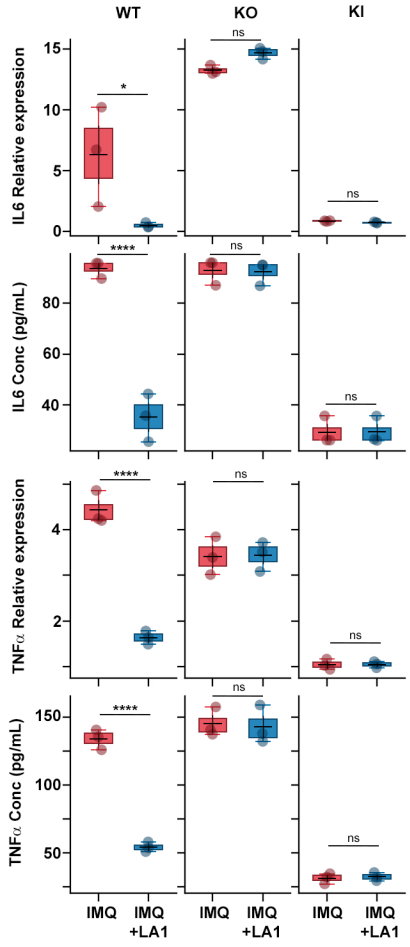

c. Pharmacologic and genetic activation of CD11b suppresses TLR4-induced inflammatory markers in BMDMs

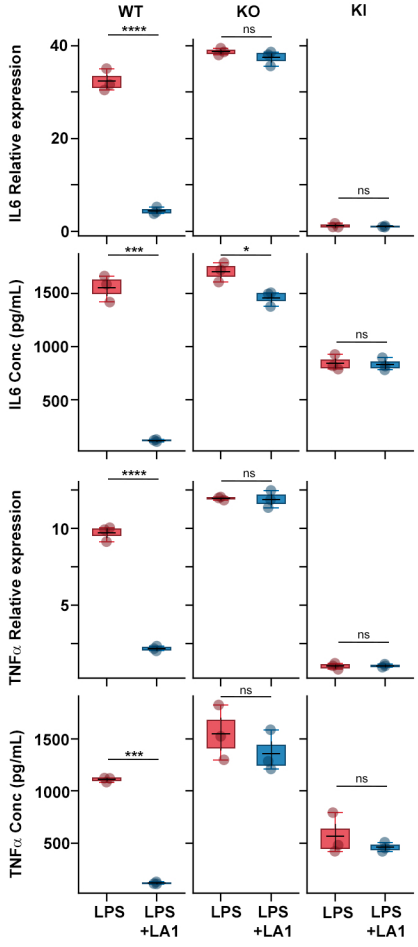

Figure S8

Figure S8. Pharmacologic and genetic activation of CD11b suppresses TLR-induced inflammatory outputs in bone-marrow-derived macrophages. a. Relative *Plaur* expression and secreted suPAR in bone-marrow-derived macrophages (BMDMs) from wild-type (WT), CD11b-deficient (KO), and active-state CD11b I332G knock-in (KI) mice stimulated with LPS (50 ng/ml) in the absence or presence of LA1 (20 μM). **b.** IL-6 and TNFα transcript and protein levels in WT, KO, and KI BMDMs stimulated with IMQ (20 μg/ml) in the absence or presence of LA1 (20 μM). **c.** IL-6 and TNFα transcript and protein levels in WT, KO, and KI BMDMs stimulated with LPS (50 ng/ml) in the absence or presence of LA1 (20 μM). Data show mean ± s.e.m. (n = 3). ns, not significant; one, two, three, and four asterisks denote $P < 0.05$, $P < 0.01$, $P < 0.001$, and $P < 0.0001$, respectively. Comparisons between two groups used two-tailed unpaired t-tests with Welch's correction and among three or more groups used one-way ANOVA with Tukey's multiple-comparison test.

a. RAW WB

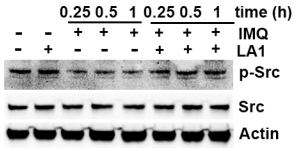

b. RAW Cell WB Quantification

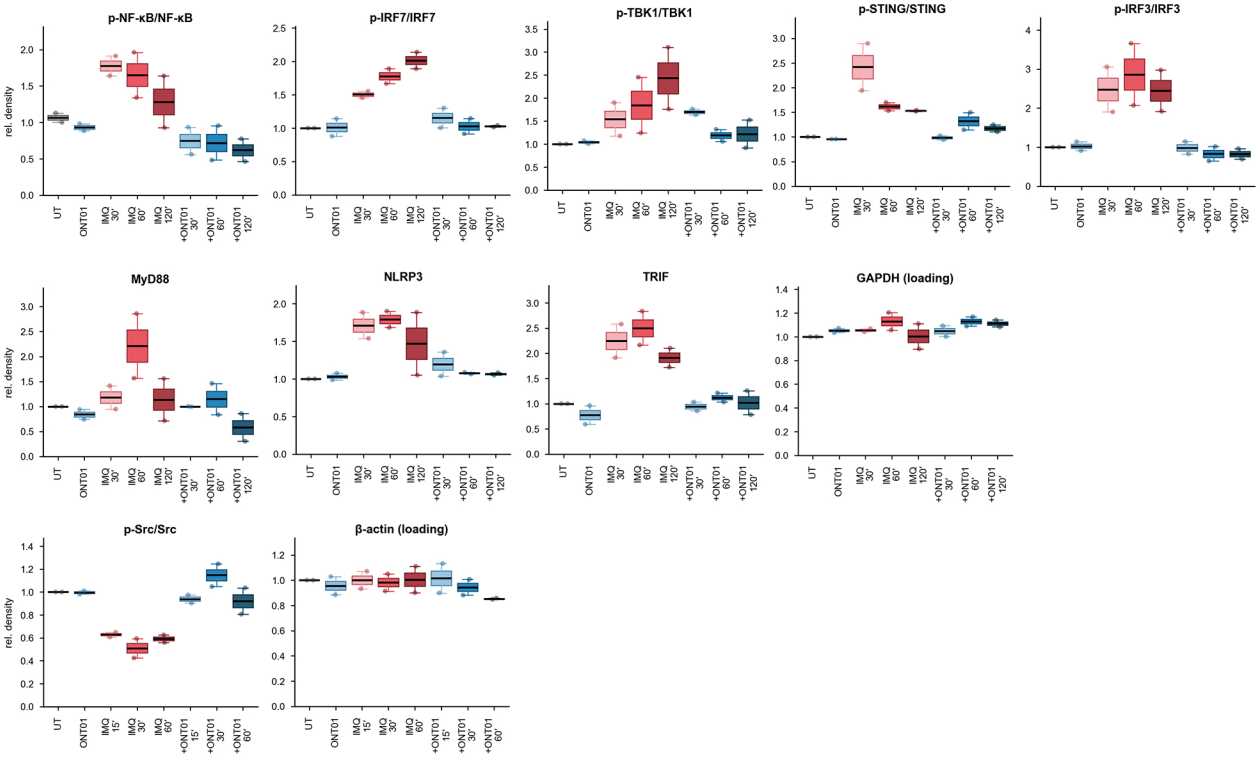

Figure S9

Figure S9. Quantification of CD11b-dependent TLR7 signaling in RAW264.7 macrophages. a. Representative immunoblots of phosphorylated and total Src in RAW 264.7 macrophages stimulated with IMQ (20 μg/ml) in the absence or presence of LA1 (20 μM) for 0.25, 0.5, or 1 h. Untreated and LA1-only controls are shown. Actin was used as a loading control. **b.** Normalized densitometric values corresponding to the immunoblots in Fig. 4D, including phosphorylated and total p65, IRF7, TBK1, STING, and IRF3; MyD88, NLRP3, and TRIF; and phosphorylated and total Src. Cells were untreated, treated with LA1 alone (20 μM), stimulated with IMQ (20 μg/ml), or stimulated with IMQ in the presence of LA1. The p65, IRF, TBK1, STING, MyD88, NLRP3, and TRIF time courses were assessed at 0.5, 1, and 2 h; Src phosphorylation was assessed at 0.25, 0.5, and 1 h. GAPDH and actin loading-control measurements are also shown. Individual points represent independent experiments, and bars show mean ± s.e.m. ns, not significant; one, two, three, and four asterisks denote $P < 0.05$, $P < 0.01$, $P < 0.001$, and $P < 0.0001$, respectively. Comparisons between two groups used two-tailed unpaired t-tests with Welch's correction and among three or more groups used one-way ANOVA with Tukey's multiple-comparison test.

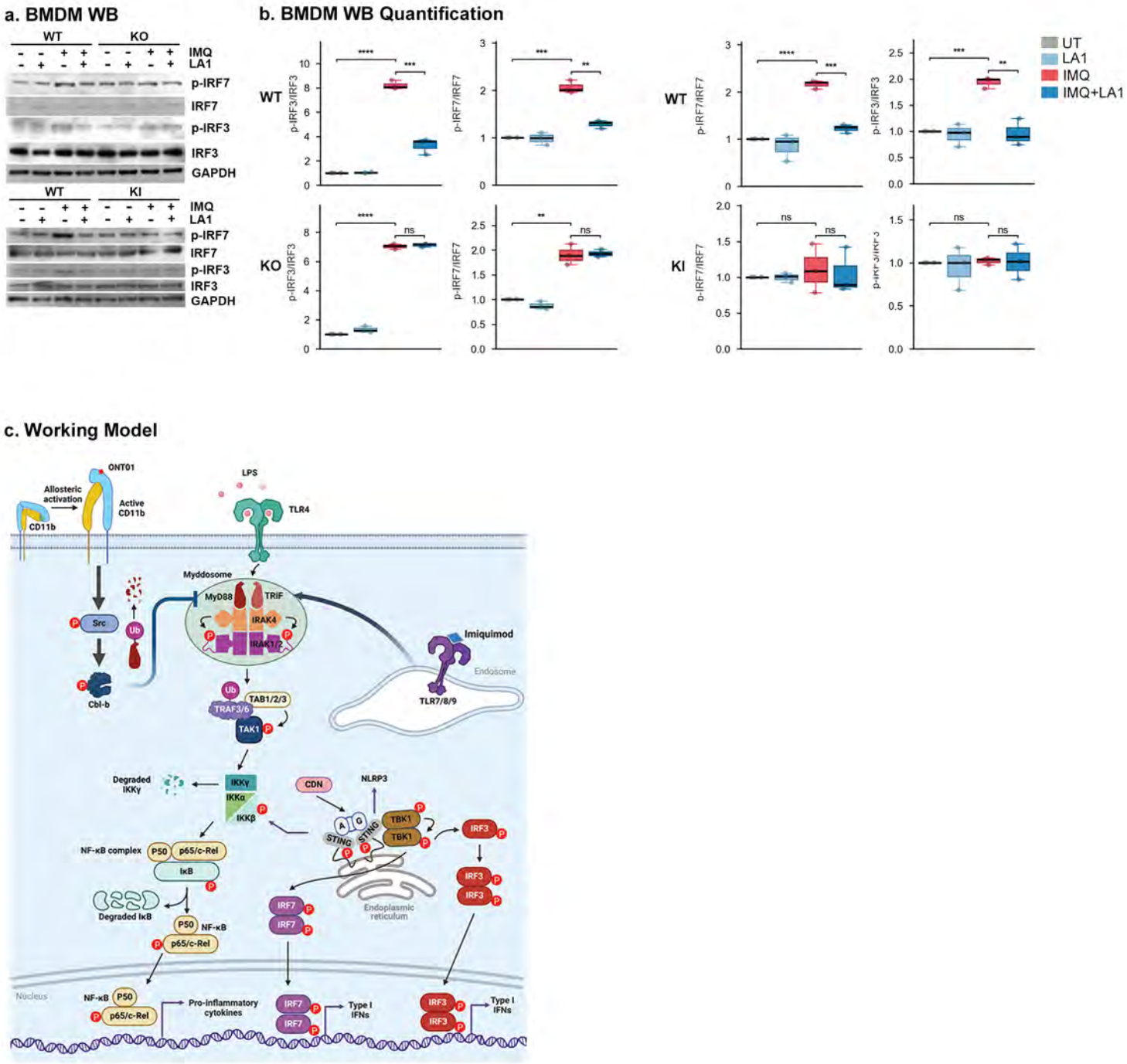
a. BMDM WB
WT
KO
IMQ
LA1
p-IRF7
IRF7
p-IRF3
IRF3
GAPDH
WT
KI
b. BMDM WB Quantification
WT
KO
p-IRF3/IRF3
p-IRF7/IRF7
UT
LA1
IMQ
IMQ+LA1
KI
ns
c. Working Model
ONT01
Allosteric activation
Active CD11b
CD11b
LPS
TLR4
Myddosome
MyD88
TRIF
IRAK4
IRAK1/2
Src
Ub
Cbl-b
Imiquimod
Endosome
TLR7/8/9
TAB1/2/3
TRAF3/6
TAK1
Degraded IKKγ
IKKγ
IKKα
IKKβ
CDN
NLRP3
STING
TBK1
IRF3
NF-κB complex
P50
p65/c-Rel
IκB
Degraded IκB
NF-κB
Endoplasmic reticulum
IRF7
Nucleus
Pro-inflammatory cytokines
Type I IFNs

Figure S10

Figure S10. CD11b conformational state regulates IMQ-induced IRF3 and IRF7 phosphorylation. **a.** Representative immunoblots of phosphorylated and total IRF7 and IRF3 in WT and KO BMDMs (top) and WT and KI BMDMs (bottom) treated with IMQ (20 μg/ml) in the absence or presence of LA1 (20 μM) for 1 h. GAPDH was used as a loading control. Immunoblots are representative of at least three independent experiments. **b.** Densitometric ratios of phosphorylated to total IRF3 and IRF7 in (left) WT and CD11b-deficient BMDMs and in (right) WT and active-state CD11b I332G knock-in BMDMs. Cells were untreated, treated with LA1 alone (20 μM), stimulated with IMQ (20 μg/ml), or stimulated with IMQ in the presence of LA1 for 1 h. Individual points represent independent experiments, and bars show mean ± s.e.m. **c.** Proposed working model in which CD11b activation promotes proximal suppression of TLR-adapter signaling and limits downstream NF-κB- and IRF-dependent inflammatory outputs. ns, not significant; two, three, and four asterisks denote $P < 0.01$, $P < 0.001$, and $P < 0.0001$, respectively. Comparisons between two groups used two-tailed unpaired t-tests with Welch's correction and among three or more groups used one-way ANOVA with Tukey's multiple-comparison test.

Primary KI macrophage treatment

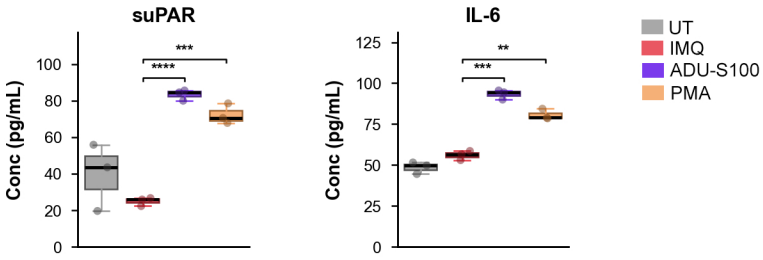

Figure S11

Figure S11. Direct STING or PKC activation induces inflammatory outputs in active-state CD11b knock-in macrophages. ELISA-based quantification of suPAR and IL-6 in supernatants from primary BMDMs from active-state CD11b I332G knock-in mice treated for 4 h with vehicle (UT), IMQ [20 μg/ml], the STING agonist ADU-S100 (1μg/mL), or the PKC activator PMA (200 ng/ml). Data show mean ± s.e.m. (n = 3). ns, not significant; three and four asterisks denote $P < 0.001$ and $P < 0.0001$, respectively. Comparisons between two groups used two-tailed unpaired t-tests with Welch's correction and among three or more groups used one-way ANOVA with Tukey's multiple-comparison test.

Mouse spleen_IMQ model

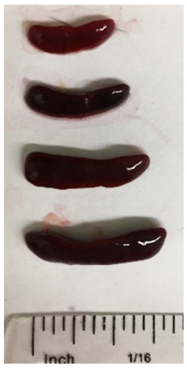

UT

IMQ+ONT01

IMQ+Veh

IMQ

Figure S12

Figure S12. Representative spleens from the IMQ-induced lupus model. Representative endpoint images of whole spleens from untreated mice (UT), IMQ-treated mice receiving ONT01, IMQ-treated mice receiving vehicle, and mice treated with IMQ alone. A ruler is shown for scale.

a. Myeloid Cell Kidney Panel Gating Strategy

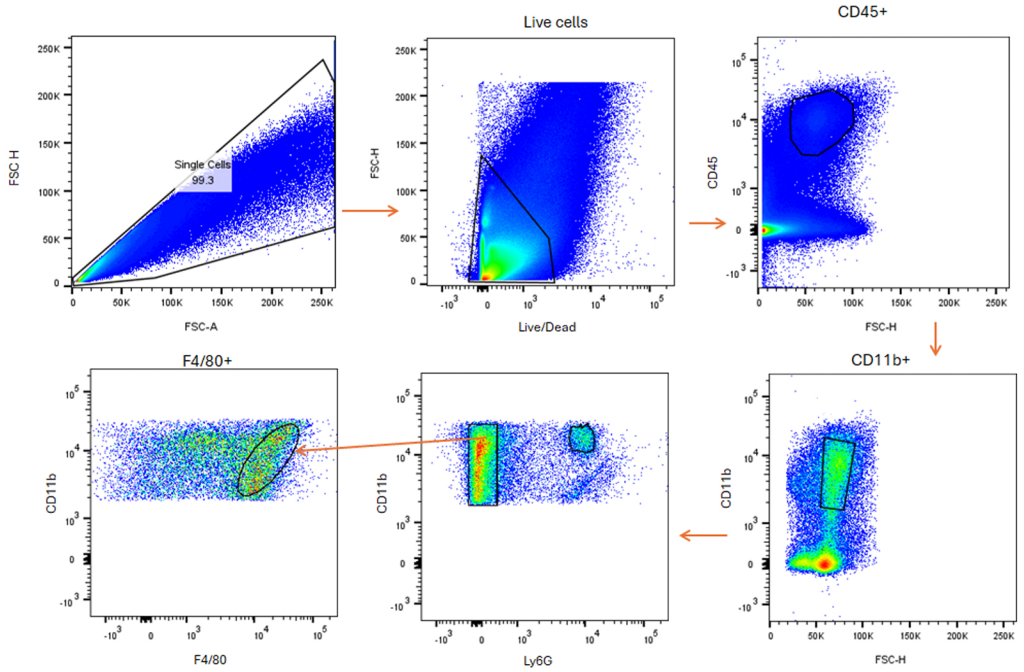

b. Lymphoid Cell Kidney Panel Gating Strategy

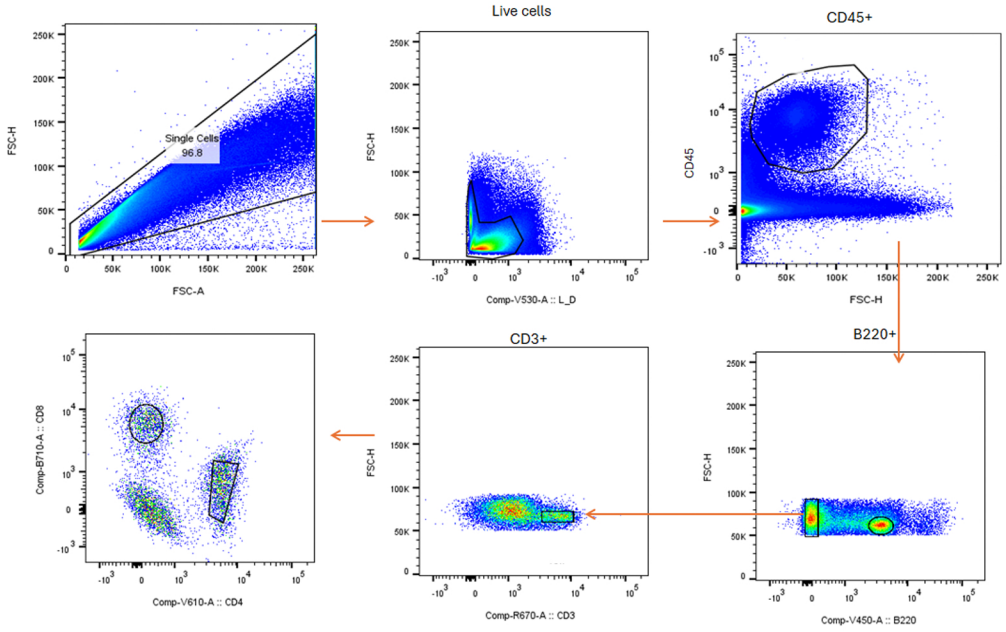

Figure S13

Figure S13. Kidney flow-cytometry gating strategies. a. Representative gating strategy for renal myeloid populations. Singlets and live cells were gated sequentially, followed by $CD45^+$ leukocytes and $CD11b^+$ myeloid cells; $Ly6G^+$ granulocytes and $F4/80^+$ macrophages were subsequently identified. **b.** Representative gating strategy for renal lymphoid populations. Singlets, live cells, and $CD45^+$ leukocytes were gated sequentially, followed by $B220^+$ B cells and $CD3^+$ T cells; $CD4^+$ and $CD8^+$ T-cell subsets were then identified.

a. Aged B Cell Spleen Panel Gating Strategy

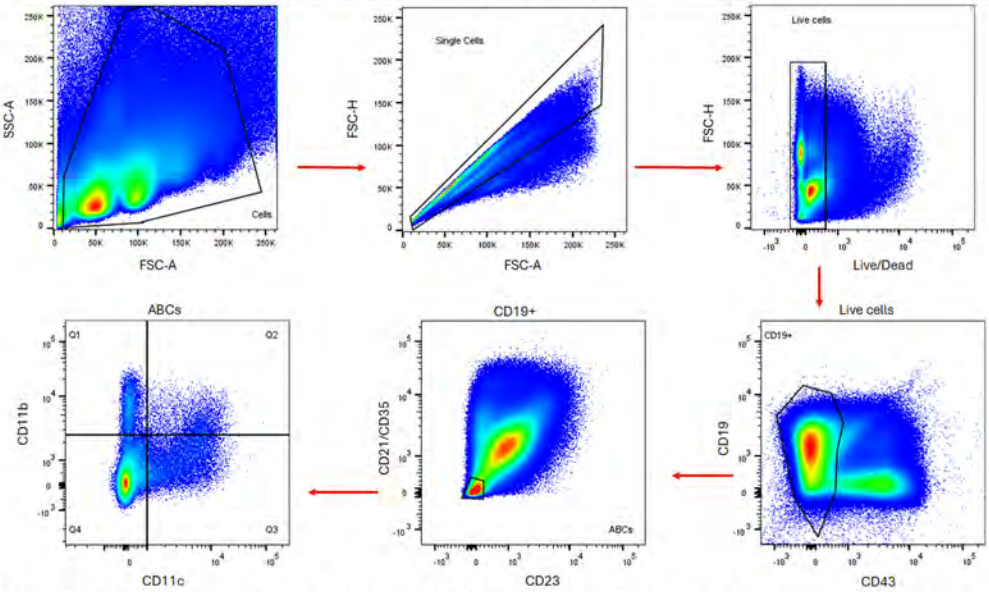

b. Aged B Cell Lymph Nodes Panel Gating Strategy

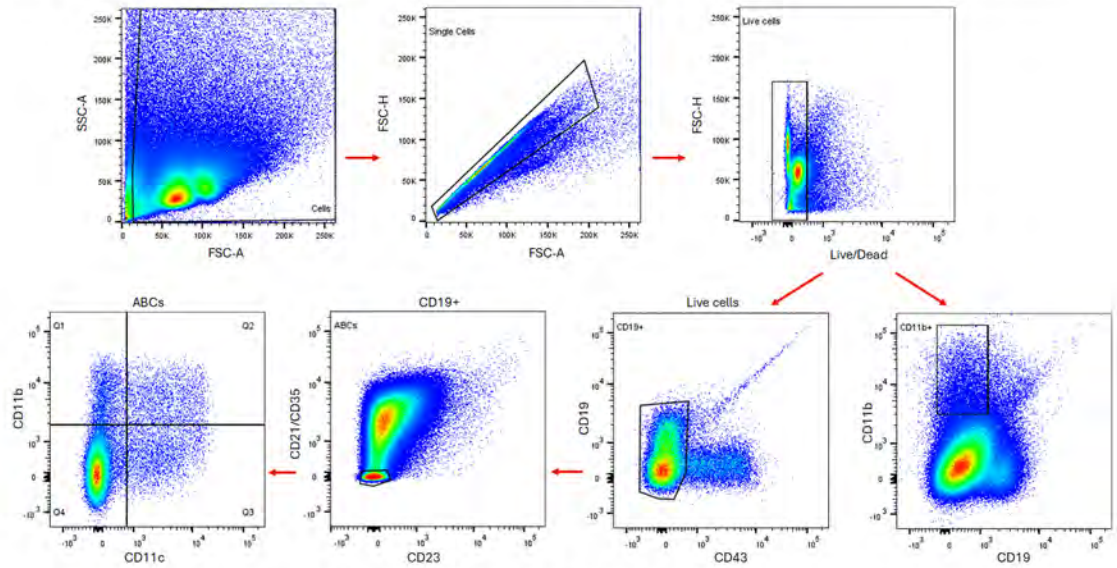

c. Aged B Cell Kidney Panel Gating Strategy

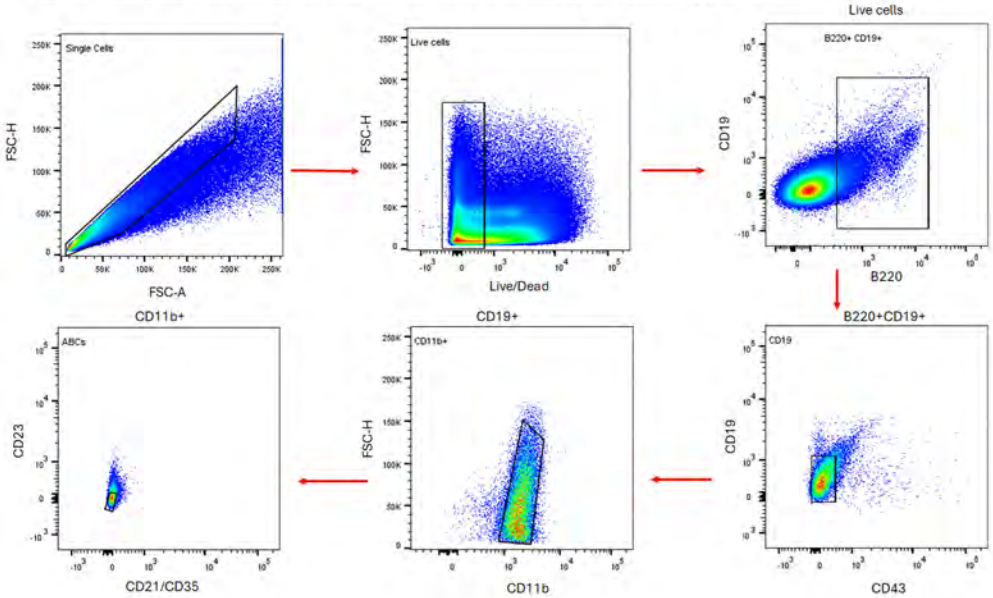

Figure S14

Figure S14. Gating strategies for age-associated B-cell analyses in spleen, lymph nodes, and kidney. Representative flow-cytometry gates used to quantify total B cells and age-associated B cells (ABCs), as operationally defined in this study. **a.** Spleen cells were gated sequentially for cells, singlets, live cells, $CD19^{+}CD43^{-}$ B cells, CD21/CD35-low CD23-low cells, and CD11b/CD11c expression. **b.** Lymph-node cells were gated for singlets and live cells, followed by $CD11b^{+}CD19^{-}$ myeloid cells or $CD19^{+}CD43^{-}$ B cells; the B-cell population was further resolved by CD21/CD35, CD23, CD11b, and CD11c expression. **c.** Kidney cells were gated for singlets, live cells, $B220^{+}CD19^{+}$ B cells, $CD19^{+}CD43^{-}$ cells, $CD11b^{+}$ cells, and CD21/CD35-low CD23-low cells.

a. IMQ Model

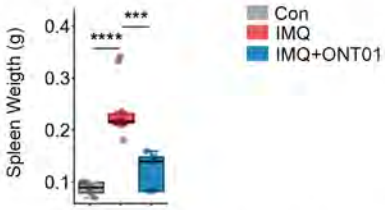

b. Histology and IHC Quantification

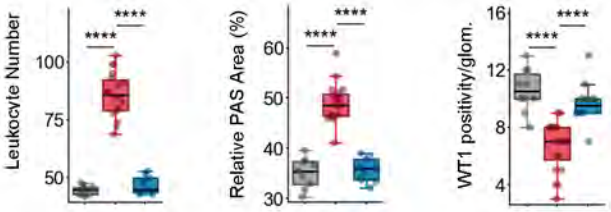

c. IF Quantification

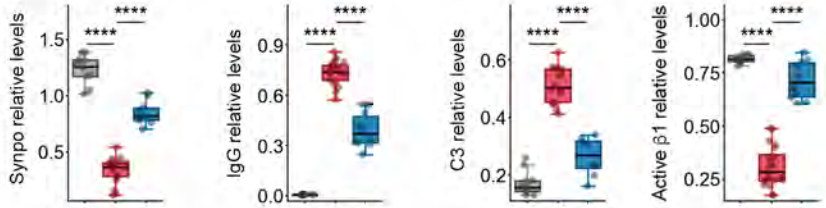

d. Flow Cytometric Quantification - kidney

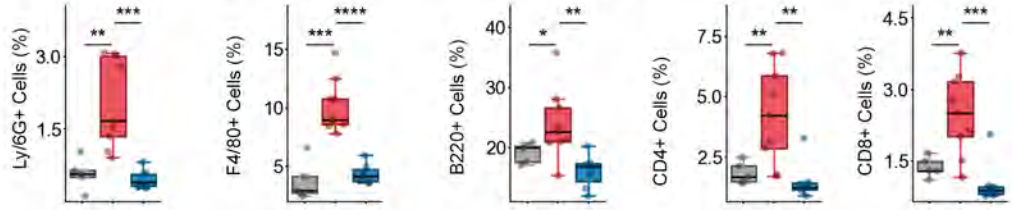

e. Myeloid IF

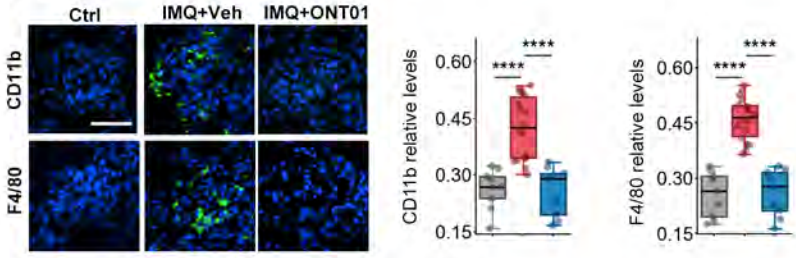

Figure S15

Figure S15. ONT01 reduces renal inflammation and injury in the IMQ-induced lupus model. a. Spleen weight in untreated controls, IMQ-treated mice receiving vehicle, and IMQ-treated mice receiving ONT01. **b.** Quantification of renal leukocyte number, relative PAS-positive area, and WT1-positive cells per glomerulus. **c.** Quantification of renal synaptopodin, IgG, C3, and active β1-integrin relative levels. **d.** Flow-cytometric quantification of renal $Ly6G^+$, $F4/80^+$, $B220^+$, $CD4^+$, and $CD8^+$ cells. **e.** Representative renal immunofluorescence for CD11b and F4/80 and corresponding relative-level quantification. Each point represents one mouse; boxplots show the median and interquartile range. ns, not significant; one, two, three, and four asterisks denote $P < 0.05$, $P < 0.01$, $P < 0.001$, and $P < 0.0001$, respectively. Comparisons between two groups used two-tailed unpaired t-tests with Welch's correction and among three or more groups used one-way ANOVA with Tukey's multiple-comparison test.

a. Spleen

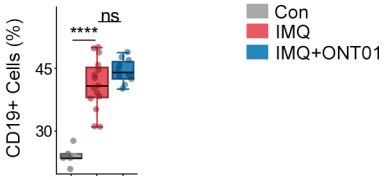

b. Lymph Nodes

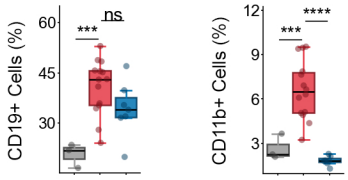

c. Migration assay

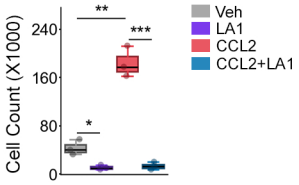

Figure S16

Figure S16. ONT01 treatment reduces CD11b^{+} ABCs in IMQ-treated mice and CCL2-dependent transmigration of cells. a. Total CD19^{+} B cells as a percentage of live splenic cells in untreated controls, IMQ-treated mice, and IMQ-treated mice receiving ONT01. Control, n = 5; IMQ, n = 15; IMQ plus ONT01, n = 10. **b.** Total CD19^{+} B cells and CD11b^{+}CD19^{-} cells as percentages of live lymph-node cells. Control, n = 3; IMQ, n = 14; IMQ plus ONT01, n = 7. Each point represents one mouse, and bars show mean ± s.e.m. ns, not significant; two and four asterisks denote $P < 0.01$ and $P < 0.0001$, respectively. **c.** Transwell migration of THP-1 human monocytes (5×10^5 cells) placed in the upper chamber in the presence of vehicle or LA1 (20 μM), with control medium or CCL2 (50 ng/ml) in the lower chamber. Data show mean ± SEM (n = 3 per group). Comparisons between two groups used two-tailed unpaired t-tests with Welch's correction and among three or more groups used one-way ANOVA with Tukey's multiple-comparison test.

a. Mrl/lpr Model - Histology and IHC Quantification

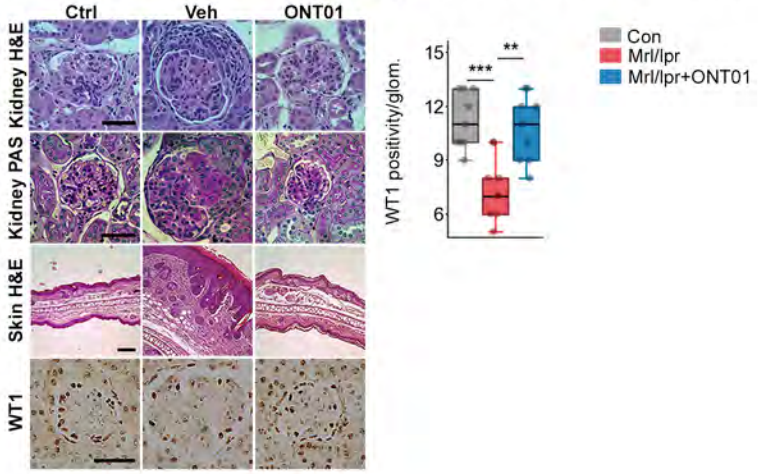

b. IF and Quantification

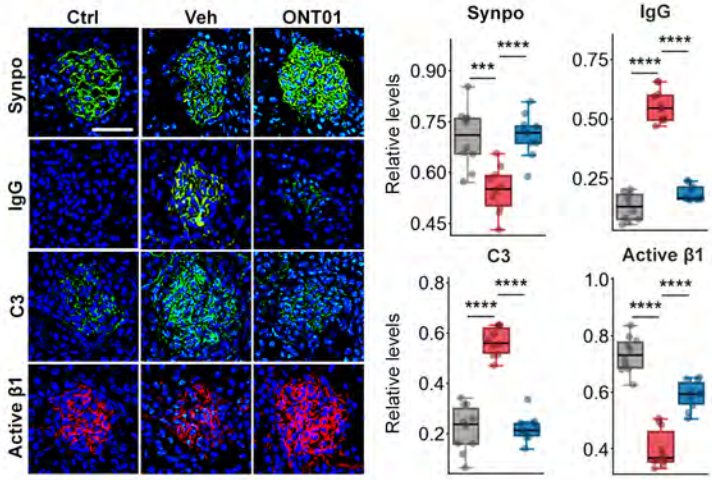

c. Myeloid IF

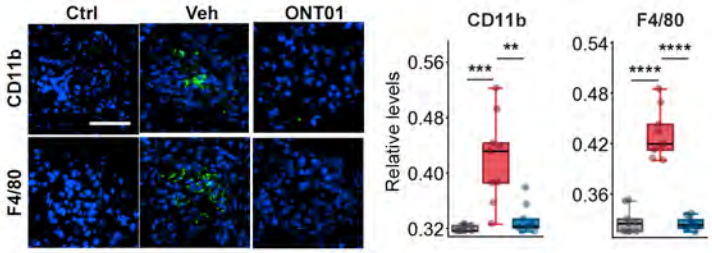

Figure S17

Figure S17. ONT01 reduces tissue injury and renal myeloid accumulation in MRL/lpr mice. a. Representative kidney H&E and PAS staining, skin H&E staining, and kidney WT1 immunohistochemistry in control MRL/mpj mice, vehicle-treated MRL/lpr mice, and ONT01-treated MRL/lpr mice, with quantification of WT1-positive cells per glomerulus. **b.** Representative renal immunofluorescence for synaptopodin, IgG, C3, and active β1 integrin and corresponding relative-level quantification. **c.** Representative renal immunofluorescence for CD11b and F4/80 and corresponding relative-level quantification. Each point represents one mouse; boxplots show the median and interquartile range. Two, three, and four asterisks denote $P < 0.01$, $P < 0.001$, and $P < 0.0001$, respectively. Comparisons between two groups used two-tailed unpaired t-tests with Welch's correction and among three or more groups used one-way ANOVA with Tukey's multiple-comparison test.

a. KO/KI IMQ Model Histology and IHC Quantification

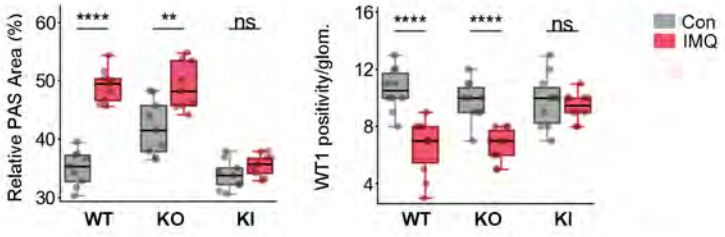

b. IF Quantification

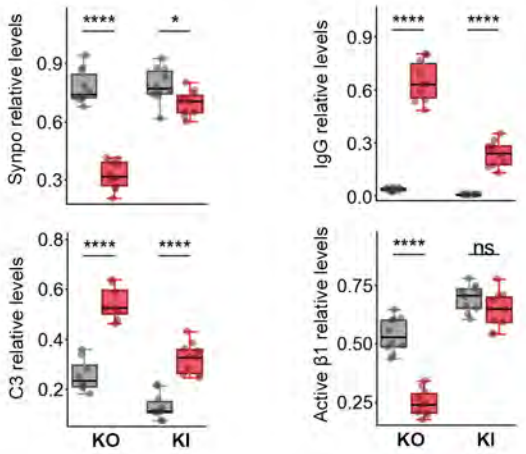

c. Myeloid IF

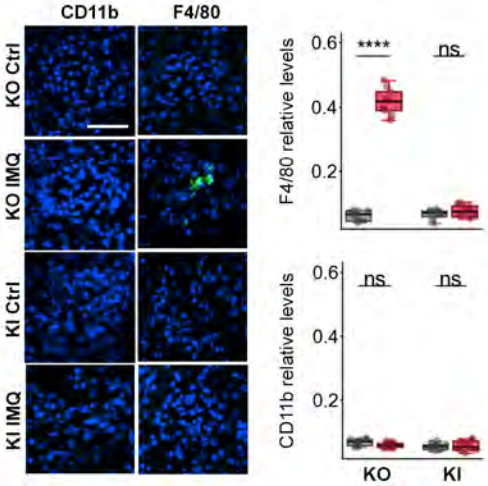

Figure S18

Figure S18. Renal pathology in wild-type, CD11b-deficient, and active-state CD11b knock-in mice following IMQ challenge. a. Relative renal PAS-positive area and WT1-positive cells per glomerulus in untreated and IMQ-treated WT, CD11b-deficient (KO), and active-state CD11b I332G knock-in (KI) mice. **b.** Quantification of renal synaptopodin, IgG, C3, and active β1-integrin relative levels in untreated and IMQ-treated KO and KI mice. **c.** Representative renal immunofluorescence for CD11b and F4/80 in untreated and IMQ-treated KO and KI mice, with corresponding quantification. Each point represents one mouse. ns, not significant; one, two, and four asterisks denote $P < 0.05$, $P < 0.01$, and $P < 0.0001$, respectively. Comparisons between two groups used two-tailed unpaired t-tests with Welch's correction and among three or more groups used one-way ANOVA with Tukey's multiple-comparison test.

a. Humanized LN mouse model

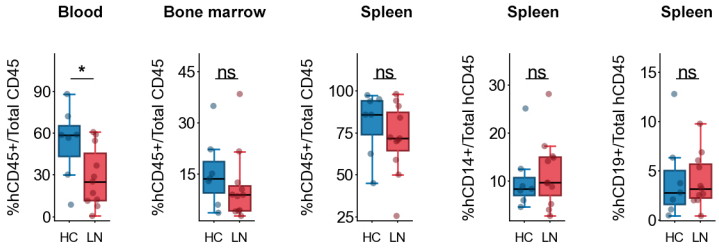

b. Serum

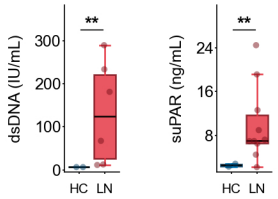

c. Spleen

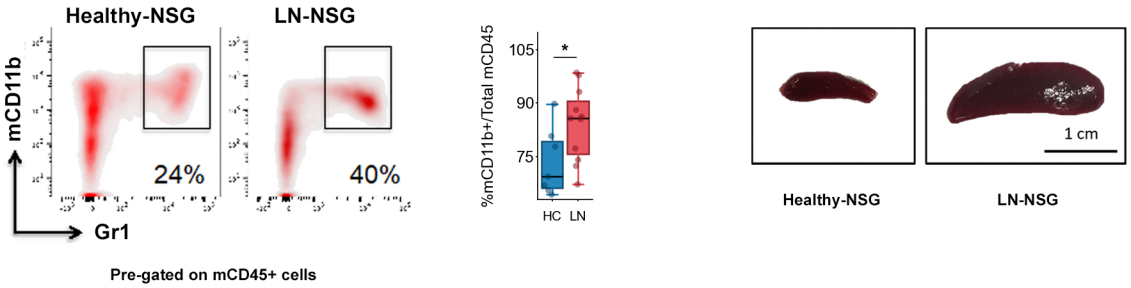

Figure S19

Figure S19. Characterization of the lupus nephritis PBMC-engrafted NSG model. a. Human-cell engraftment in blood, bone marrow, and spleen of NSG mice receiving healthy-control (HC) or lupus nephritis (LN) PBMCs. Graphs show human $CD45^+$ cells as a fraction of total $CD45^+$ cells in blood, bone marrow, and spleen, and human $CD14^+$ and $CD19^+$ cells as fractions of splenic human $CD45^+$ cells. **b.** Serum anti-dsDNA antibodies and suPAR in HC and LN PBMC recipients. **c.** Representative flow-cytometry plots of host murine $Gr1^+CD11b^+$ splenocytes, quantification of murine $CD11b^+$ cells among murine $CD45^+$ splenocytes, and representative whole spleens from HC and LN PBMC recipients. Scale bar, 1 cm. Each point represents one recipient, and bars show mean ± s.e.m. ns, not significant; one and two asterisks denote $P < 0.05$ and $P < 0.01$, respectively. Comparisons between two groups used two-tailed unpaired t-tests with Welch's correction and among three or more groups used one-way ANOVA with Tukey's multiple-comparison test.

a. TLRa IMQ driven model with delayed ONT01 Treatment

Serum

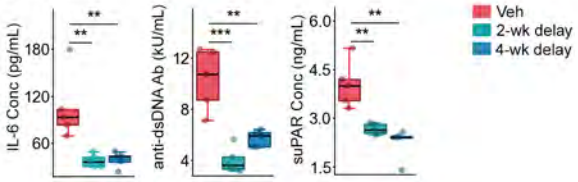

Tissue

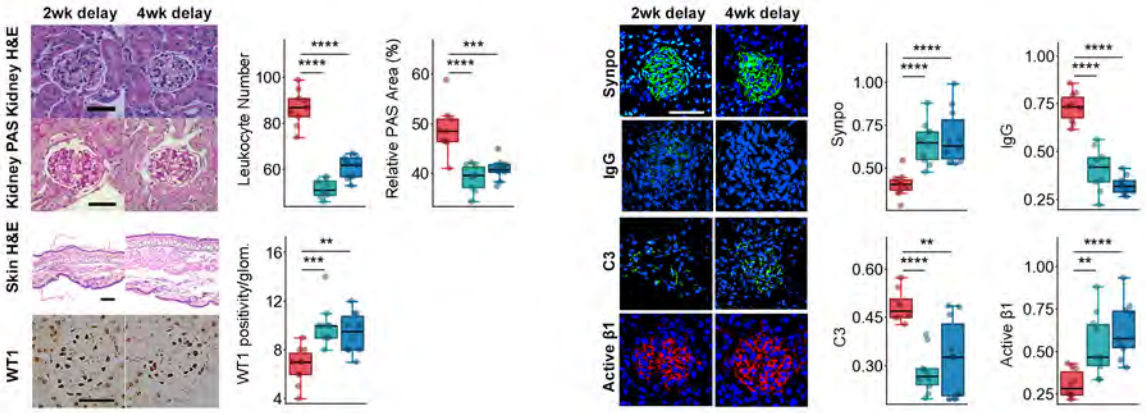

b. Mrl/lpr LN model with delayed ONT01 Treatment

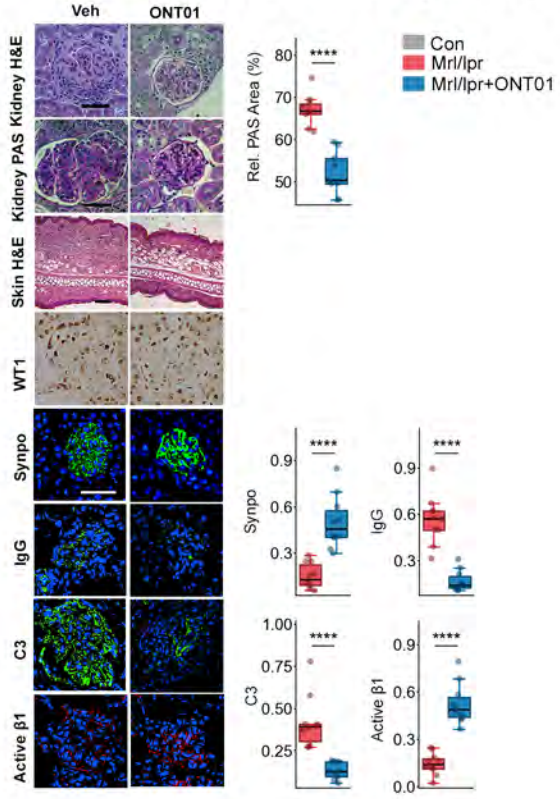

Figure S20

Figure S20. Therapeutic treatment with ONT01 reduces tissue injury and renal myeloid accumulation in two LN models. a. Data from IMQ-induced TLR7 lupus nephritis model with therapeutic ONT01 treatment, with treatment initiated 2 or 4 weeks after IMQ induction. Serum. Graphs showing end-point quantification of serum IL-6, anti-dsDNA Ab and suPAR levels in various treatment groups, as labeled (controls are same as controls in Fig 4H). Data show mean ± SEM (n = 6 per group). Tissue. (left) Representative kidney H&E and PAS staining, skin H&E staining, and kidney WT1 immunohistochemistry in delayed ONT01-administered mice in this IMQ LN model, with treatment initiated 2 or 4 weeks after IMQ induction (as labeled). (Scale bar: 50 μm). Quantification of various markers is shown next to the images. (right) Representative renal immunofluorescence for synaptopodin, IgG, C3, and active β1 integrin and corresponding relative-level quantification. Scale bar: 50 μm. b. Data from Mrl/lpr lupus nephritis model with therapeutic ONT01 treatment, with treatment initiated when mice reached 10 weeks of age. (top panels) Representative kidney H&E and PAS staining, skin H&E staining, and kidney WT1 immunohistochemistry in delayed ONT01-administered mice in this LN model (as labeled). Scale bar: 50 μm. Quantification of various markers is shown next to the images. (bottom panels) Representative renal immunofluorescence for synaptopodin, IgG, C3, and active β1 integrin and corresponding relative-level quantification. Scale bar: 50 μm. Quantitative panels show individual biological replicates with mean ± SEM or boxplot summaries, as displayed. ns, not significant; two, three, and four asterisks denote $P < 0.01$, $P < 0.001$, and $P < 0.0001$, respectively. Comparisons between two groups used two-tailed unpaired t-tests with Welch's correction and among three or more groups used one-way ANOVA with Tukey's multiple-comparison test.

Human Clinical Trial Design for PK and Safety Assessment of ONT01

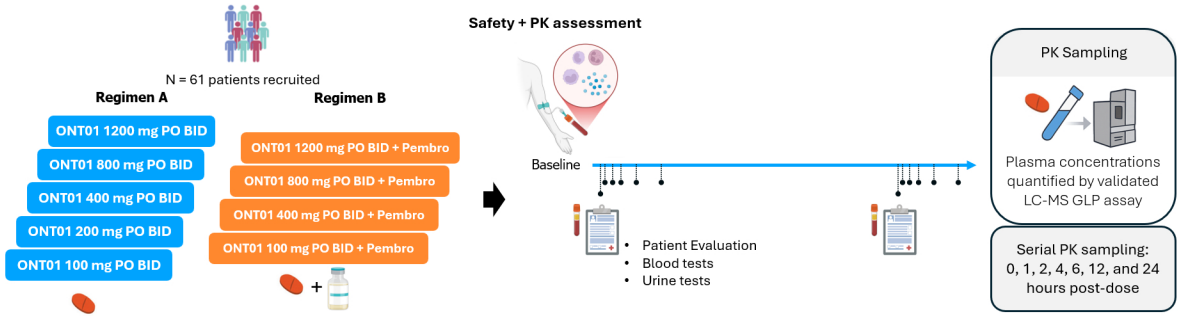

Figure S21

Figure S21. First-in-human clinical trial study design for study of ONT01. A schematic showing the clinical trial design for testing ONT01 in a recently completed multi-center Phase I safety and PK study in patients (ClinicalTrials.gov ID: NCT04060342). The dose-escalation phase utilized a standard 3+3 design and assessed BID administration of ONT01 either as a monotherapy (Regimen A) or in combination with an anti-PD-1 antibody (Regimen B). A total of 47 subjects contributed to the pharmacokinetic (PK) data.

Model of Severe Sepsis

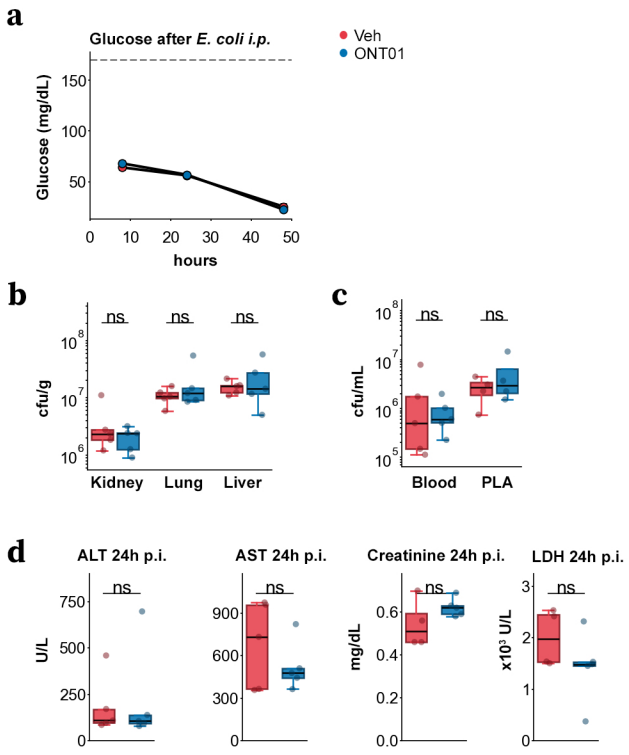

Figure S22

Figure S22. Physiological, bacterial-burden, and organ-injury measurements after high-load E. coli challenge. Mice were challenged intraperitoneally with *E. coli* K-12 and treated orally with vehicle or ONT01 [30 mg/kg] at 0 and 8 h. **a.** Blood glucose over time after infection; the dashed line indicates the reference range shown in the panel. Vehicle, n = 14; ONT01, n = 15. **b.** Bacterial burden in kidney, lung, and liver at 24 h after infection, expressed as colony-forming units (CFU) per gram. **c.** Bacterial burden in blood and peritoneal lavage fluid at 24 h, expressed as CFU per milliliter. For bacterial-burden analyses, n = 5 per group. **d.** Plasma or serum alanine aminotransferase (ALT), aspartate aminotransferase (AST), lactate dehydrogenase (LDH), and creatinine at 24 h after infection. For organ-injury measurements, n = 3–4 per group. ns, not significant. Comparisons between two groups used two-tailed unpaired t-tests with Welch's correction and among three or more groups used one-way ANOVA with Tukey's multiple-comparison test.

SLE/LN clinical trial patient criteria

Overall Inclusion Criteria

- Age ≥18
- Diagnosis of SLE criteria (ACR/EULAR criteria)
- Patients of childbearing potential: must agree to use a highly effective form of contraception during the study and for at least 120 days after last exposure to study drug
- Patients with partners of childbearing potential: must use effective barrier contraception during the study and for at least 120 days after last exposure to study drug
- Patients may not proceed with sperm or egg donation during the study and for at least 120 days after the last exposure to study drug

Active non-renal SLE

- One active non-renal clinical manifestation
- At least 1 disease modifying anti-rheumatic drug (DMARD) therapy (not including hydroxychloroquine and corticosteroids)
- Active non-renal SLE is defined as having a SLEDAI of 6 or greater (with at least 1 non-renal clinical domain)

Active nephritis

- Class III, IV, V, III+V, or IV+V nephritis
- No or partial response after initial induction and maintenance therapy with mycophenolate mofetil (and other standard of care therapies) for 3 months
- 24-hour urine protein/creatinine ratio >=1g/g at screening

Exclusion Criteria

- Comorbidities requiring systemic corticosteroid (CS) therapy, such as asthma or inflammatory bowel disease. Systemic is defined as oral, rectal or any injectable route of administration (thus stable dosing by other routes is allowed, including inhaled, topical, ophthalmic, otic, and intranasal)
- Active central nervous system SLE associated with significant cognitive impairment
- Active chronic or acute infection
- Pregnancy (highly effective contraception must be used)
- Treatment with Voclosporin or Cyclophosphamide, or other experimental therapy within the last 3 months or 5 half-lives of the drug
- Immunization with live or live-attenuated vaccines within 1 month before or during the Screening period.
- Clinically significant abnormalities in laboratory tests, unless attributable to active SLE at the Screening Visit
    - Aspartate aminotransferase, alanine aminotransferase or alkaline phosphatase level > 2.5 × upper limit of normal (ULN), or
    - Total bilirubin > 1.5 × ULN, or
    - Hemoglobin < 5.0 mmol/L [9 g/dL], or
    - White blood cells < 2.5 × 109/L, or
    - Absolute neutrophil count < 1500 /mm3, or
    - Platelets < 75 × 109/L

Figure S23

Figure S23. Inclusion and exclusion criteria for enrolling patients in the clinical trial studying ONT01 in SLE and LN patients. Tables show detailed list of selection criteria for this clinical trial with ONT01 in SLE and LN patients.

Supplementary Tables

Table S1. 5 trans-eQTL targets of the ITGAM R77H coding allele in eQTLGen (N=31,684 blood samples)

Gene	ISG	Best sentinel SNP	r2 to R77H	Z	P	FDR	Direction
RSAD2	Y	rs9888739	0.911	5.6549	1.560E-08	1.581E-04	up
SSBP4	N	rs1143679	1	-4.7961	1.617E-06	1.066E-02	down
IFI44	Y	rs11860650	0.903	4.7932	1.643E-06	1.085E-02	up
HERC5	Y	rs11860650	0.903	4.7031	2.564E-06	1.592E-02	up
IFI44L	Y	rs11860650	0.903	4.6539	3.259E-06	1.967E-02	up

Table S2. 47 trans signals at the ITGAM locus attributable to the neighboring VKORC1/KAT8 cluster, not the R77H coding allele (eQTLGen, N=31,684 blood samples)

Gene	Best SNP	Class	Z	P	FDR
GUCD1	rs12445568	neighbour-attributable (VKORC1/KAT8 region)	6.7243	1.766E-11	0.000E+00
ANKRD55	rs11649653	neighbour-attributable (VKORC1/KAT8 region)	6.5074	7.656E-11	0.000E+00
CAMK2N1	rs74249949	neighbour-attributable (VKORC1/KAT8 region)	6.3165	2.677E-10	0.000E+00
CYBRD1	rs749671	neighbour-attributable (VKORC1/KAT8 region)	-6.247	4.184E-10	1.777E-05
CACNA1I	rs11649653	neighbour-attributable (VKORC1/KAT8 region)	6.2368	4.466E-10	1.764E-05
C19orf77	rs13708	neighbour-attributable (VKORC1/KAT8 region)	5.9778	2.265E-09	6.214E-05
DPCD	rs12445568	neighbour-attributable (VKORC1/KAT8 region)	5.7859	7.217E-09	1.265E-04
APBA2	rs10782001	neighbour-attributable (VKORC1/KAT8 region)	-5.5705	2.539E-08	2.770E-04
CDH2	rs13708	neighbour-attributable (VKORC1/KAT8 region)	5.4034	6.539E-08	7.072E-04
PPP2R5B	rs13708	neighbour-attributable (VKORC1/KAT8 region)	5.3865	7.188E-08	7.566E-04
FAM108C1	rs74249949	neighbour-attributable (VKORC1/KAT8 region)	5.2236	1.757E-07	1.470E-03
RP11-664D1.1	rs13708	neighbour-attributable (VKORC1/KAT8 region)	-5.1735	2.296E-07	1.870E-03
AXIN2	rs13708	neighbour-attributable (VKORC1/KAT8 region)	-5.0795	3.782E-07	2.868E-03
KRT72	rs10782001	neighbour-attributable (VKORC1/KAT8 region)	-5.0545	4.313E-07	3.287E-03
INTS3	rs9925964	neighbour-attributable (VKORC1/KAT8 region)	-5.0391	4.675E-07	3.492E-03
KRT1	rs10871454	neighbour-attributable (VKORC1/KAT8 region)	5.0133	5.353E-07	3.976E-03
NINJ2	rs749671	neighbour-attributable (VKORC1/KAT8 region)	4.9849	6.203E-07	4.610E-03
ELOVL4	rs11649653	neighbour-attributable (VKORC1/KAT8 region)	-4.8683	1.125E-06	7.585E-03
POLD4	rs12445568	neighbour-attributable (VKORC1/KAT8 region)	4.8075	1.529E-06	1.006E-02
SHARPIN	rs12445568	neighbour-attributable (VKORC1/KAT8 region)	4.8065	1.537E-06	1.009E-02
AFAP1L2	rs74249949	neighbour-attributable (VKORC1/KAT8 region)	4.8044	1.554E-06	1.025E-02
BZRAP1	rs9923231	neighbour-attributable (VKORC1/KAT8 region)	4.7948	1.630E-06	1.074E-02
KRT73	rs13708	neighbour-attributable (VKORC1/KAT8 region)	-4.7895	1.671E-06	1.097E-02
FXYD2	rs12445568	neighbour-attributable (VKORC1/KAT8 region)	-4.7715	1.828E-06	1.196E-02
ZNF285	rs7197475	neighbour-attributable (VKORC1/KAT8 region)	-4.7476	2.058E-06	1.339E-02
PVT1	rs9923231	neighbour-attributable (VKORC1/KAT8 region)	4.7222	2.333E-06	1.478E-02
PARP3	rs12445568	neighbour-attributable (VKORC1/KAT8 region)	4.7212	2.345E-06	1.479E-02
RRAGD	rs7197475	neighbour-attributable (VKORC1/KAT8 region)	4.7067	2.519E-06	1.564E-02
PDZK1IP1	rs13708	neighbour-attributable (VKORC1/KAT8 region)	-4.7033	2.559E-06	1.591E-02
RNF187	rs13708	neighbour-attributable (VKORC1/KAT8 region)	4.6414	3.464E-06	2.073E-02
NT5E	rs11649653	neighbour-attributable (VKORC1/KAT8 region)	-4.6369	3.535E-06	2.109E-02
RRAS	rs11649653	neighbour-attributable (VKORC1/KAT8 region)	-4.6271	3.706E-06	2.193E-02
NET1	rs7197475	neighbour-attributable (VKORC1/KAT8 region)	-4.6093	4.038E-06	2.348E-02
SNX17	rs12445568	neighbour-attributable (VKORC1/KAT8 region)	4.5687	4.910E-06	2.756E-02
KCTD15	rs74249949	neighbour-attributable (VKORC1/KAT8 region)	4.5647	5.005E-06	2.798E-02
CSGALNACT1	rs10782001	neighbour-attributable (VKORC1/KAT8 region)	-4.5498	5.365E-06	2.960E-02
FAM214B	rs13708	neighbour-attributable (VKORC1/KAT8 region)	4.5321	5.843E-06	3.191E-02
TRIM41	rs10782001	neighbour-attributable (VKORC1/KAT8 region)	4.529	5.926E-06	3.236E-02
TADA3	rs10782001	neighbour-attributable (VKORC1/KAT8 region)	4.5195	6.202E-06	3.352E-02
CCDC14	rs10782001	neighbour-attributable (VKORC1/KAT8 region)	4.5192	6.207E-06	3.356E-02
MAN1C1	rs13708	neighbour-attributable (VKORC1/KAT8 region)	-4.5009	6.764E-06	3.588E-02
MMP28	rs13708	neighbour-attributable (VKORC1/KAT8 region)	-4.4991	6.821E-06	3.616E-02
WDR54	rs12445568	neighbour-attributable (VKORC1/KAT8 region)	4.4969	6.898E-06	3.648E-02
HEPACAM2	rs13708	neighbour-attributable (VKORC1/KAT8 region)	-4.4838	7.333E-06	3.826E-02
C17orf62	rs9925964	neighbour-attributable (VKORC1/KAT8 region)	-4.4697	7.829E-06	4.046E-02
BSCL2	rs74249949	neighbour-attributable (VKORC1/KAT8 region)	4.4666	7.955E-06	4.108E-02
SIGLEC9	rs74249949	neighbour-attributable (VKORC1/KAT8 region)	-4.4144	1.012E-05	4.928E-02

Table S1. 5 trans-eQTL targets of the *ITGAM* R77H coding allele in eQTLGen (N=31,684 blood samples).

Table S3. Coding (R77H) versus regulatory haplotype dissociation at the ITGAM locus: cis CD11b abundance versus trans interferon-stimulated genes

Arm	Lead variant	Annotation	cis: CD11b abundance (bet	cis P	cis credible set	trans: ISGs (N at FDR<0.05	trans lead (Z)	trans credible set
Coding (R77H conformational)	rs1143679	R77H missense	-0.0041	6.800E-01	absent (GTEx SuSiE 0/50)	5	RSAD2 (5.65)	present
Regulatory (receptor quantity)	rs3087796	3'UTR regulatory lead	-0.1506	7.380E-122	present (dominant)	0	—	absent

LD between leads: r2 = 0.073, D' = 0.9999 (1000 Genomes phase 3 EUR, Ensembl REST). Low r2 governs statistical separability; high D' reflects the allele-frequency offset between leads.
Regulatory cis-pQTL measured at tag rs59338016 (r2 ~ 1.0 to rs3087796; UKB-PPP+SCALLOP). Coding cis-pQTL (CD11b abundance) is null; regulatory arm carries no interferon-stimulated trans-eQTL.

Table S2. 47 trans signals at the *ITGAM* locus attributable to the neighboring VKORC1/KAT8 cluster, not the R77H coding allele (eQTLGen, N=31,684 blood samples).

Table S4. Engagement of the 21-gene type-I interferon signature by the ITGAM R77H coding allele in eQTLGen (N=31,684 blood samples)

Gene	Z	Direction	P	Genome-wide FDR
RSAD2	5.111	up	3.211E-07	0.0025
HERC5	4.42	up	9.879E-06	0.0484
IFI44L	4.186	up	2.842E-05	0.1067
IFI44	4.144	up	3.407E-05	0.1207
OAS2	4.01	up	6.072E-05	0.1771
OAS3	3.989	up	6.641E-05	0.1874
EPSTI1	3.946	up	7.953E-05	0.2084
IFIT3	3.589	up	3.317E-04	0.424
MX1	3.511	up	4.468E-04	0.474
IFI6	3.413	up	6.430E-04	0.5339
IFIT1	3.191	up	1.421E-03	0.6506
SIGLEC1	3.026	up	2.481E-03	0.72
LY6E	2.997	up	2.730E-03	0.7303
USP18	2.629	up	8.559E-03	0.8319
ISG15	2.291	up	2.197E-02	0.8899
OAS1	2.083	up	3.723E-02	0.9144
LAMP3	1.389	up	1.650E-01	0.964
IFI27	1.183	up	2.367E-01	0.9732
PLSCR1	1.17	up	2.420E-01	0.9737
PARP9	0.053	up	9.581E-01	1
RTP4	-0.279	down	7.799E-01	0.9966

Table S3. Coding (R77H) versus regulatory haplotype dissociation at the *ITGAM* locus: cis CD11b abundance versus trans interferon-stimulated genes.

Table S5. Plasma protein trans-pQTL program of the *ITGAM* R77H coding haplotype

Protein	Program	Effect (β)	q (FDR)	Plasma class
BST2	IFN-induced secreted	0.068559	8.218E-10	credible
SIGLEC1	macrophage scavenger	0.0625667	5.362E-09	credible
LGALS9	IFN-induced secreted	0.042694	7.485E-05	credible
CCL8	IFN-induced secreted	0.0325006	3.009E-03	credible
MSR1	macrophage scavenger	0.033506	5.364E-03	credible
CD163	macrophage scavenger	0.0311106	1.676E-02	credible
FCN1	macrophage scavenger	-0.0300217	1.733E-02	credible
CXCL10 ‡	IFN-induced secreted	0.0243627	6.429E-02	credible
ITGB2 †	β2 integrin partner (receptor quantity)	0.0771	3.270E-10	credible

‡ CXCL10 has program FDR q = 0.064, slightly above the 0.05 threshold. It is retained here to show a canonical type-I interferon-induced secreted marker.

† ITGB2 is the reciprocal β2 integrin chain (CD11b/CD18 heterodimer partner). The value shown is from the coding-arm (rs1143679) trans-pQTL. ITGB2 also tracks the regulatory arm (rs3087796: β = 0.118, $P = 3.6\times10^{-52}$), consistent with a receptor-quantity readout rather than the conformational interferon program.

Table S4. Engagement of the 21-gene type-I interferon signature by the *ITGAM* R77H coding allele in eQTLGen (N=31,684 blood samples)

Table S6. rs1143679 associations with IFN-related proteins after regulatory-marker adjustment

Protein	N	Additional adjustment	β	SE	Z	P value	BH-adjusted P
SIGLEC1	51,231	Marginal	0.06139	0.00942	6.517	7.18E-11	n.a.
SIGLEC1	51,231	rs3087796	0.07008	0.00975	7.191	6.43E-13	2.70E-11
SIGLEC1	51,231	rs3087796 + rs11865830	0.07098	0.00975	7.277	3.41E-13	2.70E-11
IFIT3	50,581	Marginal	0.04196	0.01041	4.032	5.53E-05	n.a.
IFIT3	50,581	rs3087796	0.04721	0.01077	4.385	1.16E-05	1.63E-04
IFIT3	50,581	rs3087796 + rs11865830	0.04738	0.01077	4.397	1.10E-05	1.63E-04
GBP1	51,209	Marginal	0.03765	0.00987	3.816	1.35E-04	n.a.
GBP1	51,209	rs3087796	0.04182	0.01021	4.098	4.17E-05	4.63E-04
GBP1	51,209	rs3087796 + rs11865830	0.04173	0.01021	4.085	4.41E-05	4.63E-04
CXCL10	51,231	Marginal	0.02436	0.00987	2.468	1.36E-02	n.a.
CXCL10	51,231	rs3087796	0.02878	0.01021	2.819	4.82E-03	2.89E-02
CXCL10	51,231	rs3087796 + rs11865830	0.02898	0.01022	2.836	4.56E-03	2.89E-02

Associations of rs1143679 (R77H) with circulating proteins in UKB-PPP. Positive effects indicate higher protein levels per A allele (reference G). β and SE retain the source protein-analysis scale. N is the source sample count for each assay and is identical across the three variants used here.

Marginal denotes the source association before additional locus conditioning. Adjusted estimates were calculated from harmonized summary statistics and signed LD from 503 European-ancestry 1000 Genomes reference individuals. These are approximate conditional estimates using external LD.

The joint model includes rs3087796 and rs11865830, representatives of distinct published ITGAM cis-regulatory credible sets. All four associations remain positive with BH-adjusted $P < 0.05$ in both adjusted models.

P values are two-sided normal-test probabilities. BH-adjusted P values retain the full 84-test protein family (28 assays × 3 planned conditional models), with unavailable tests retained in the denominator. They were not recalculated for these four proteins. n.a.: adjustment not applied to marginal P values.

β, effect estimate; SE, standard error; Z, association statistic; BH, Benjamini–Hochberg. Protein symbols identify the measured circulating proteins.

Assay identifiers (UKB-PPP)

SIGLEC1	SIGLEC1_Q9BZZ2_OID20690_v1_Inflammation
IFIT3	IFIT3_O14879_OID31283_v1_Oncology_II
GBP1	GBP1_P32455_OID31128_v1_Neurology_II
CXCL10	CXCL10_P02778_OID20697_v1_Inflammation

Table S5. Plasma protein trans-pQTL program of the *ITGAM* R77H coding haplotype.

Table S7A. AMP cohort characteristics

The AMP kidney cohort includes 155 participants with lupus nephritis (LN) and 29 controls. LN genotype groups comprise 32 R77H carriers, 95 non-carriers and 28 participants with unresolved or untyped genotype.

Values are median [Q1, Q3] or n/nonmissing N (%). Each IFN analysis reports its own sample size.

Characteristic	Overall N=184	LN n=155	Controls n=29	LN carriers n=32	LN non-carriers n=95	LN unresolved / untyped
Age, years	35 [27, 45]	33 [26, 43]	48 [35, 53]	32.5 [25.8, 44]	34 [26.5, 43.5]	31 [24.8, 39]
Sex: female	158/184 (85.9%)	135/155 (87.1%)	23/29 (79.3%)	28/32 (87.5%)	84/95 (88.4%)	23/28 (82.1%)
Sex: male	26/184 (14.1%)	20/155 (12.9%)	6/29 (20.7%)	4/32 (12.5%)	11/95 (11.6%)	5/28 (17.9%)
Reported race: Asian	25/182 (13.7%)	23/153 (15.0%)	2/29 (6.9%)	3/32 (9.4%)	17/93 (18.3%)	3/28 (10.7%)
Reported race: Black or African American	71/182 (39.0%)	67/153 (43.8%)	4/29 (13.8%)	14/32 (43.8%)	40/93 (43.0%)	13/28 (46.4%)
Reported race: Hispanic	11/182 (6.0%)	11/153 (7.2%)	0/29 (0.0%)	4/32 (12.5%)	7/93 (7.5%)	0/28 (0.0%)
Reported race: Mixed Race	3/182 (1.6%)	3/153 (2.0%)	0/29 (0.0%)	1/32 (3.1%)	2/93 (2.2%)	0/28 (0.0%)
Reported race: White	72/182 (39.6%)	49/153 (32.0%)	23/29 (79.3%)	10/32 (31.2%)	27/93 (29.0%)	12/28 (42.9%)
Reported ethnicity: Hispanic or Latino	45/184 (24.5%)	44/155 (28.4%)	1/29 (3.4%)	9/32 (28.1%)	29/95 (30.5%)	6/28 (21.4%)
Reported ethnicity: Not Hispanic or Latino	139/184 (75.5%)	111/155 (71.6%)	28/29 (96.6%)	23/32 (71.9%)	66/95 (69.5%)	22/28 (78.6%)
NIH biopsy activity index	4 [0, 8]	4 [0, 8]	Unavailable	2.5 [0, 8.75]	4 [1, 8]	2 [0, 5]
NIH biopsy chronicity index	3 [1, 5]	3 [1, 5]	Unavailable	3 [1.75, 5]	3 [1, 4]	4 [1, 6]
eGFR, CKD-EPI, mL/min/1.73 m2	90.2 [68, 117]	88.1 [63.8, 117]	106 [100, 129]	78.8 [63.7, 111]	86.5 [56.7, 116]	111 [74.6, 120]
Urine protein/creatinine ratio	1.86 [1.2, 3.3]	1.86 [1.2, 3.3]	Unavailable	2.16 [1.47, 3.64]	1.83 [1.17, 3.32]	1.47 [0.973, 2.5]

Genotype-stratified columns describe participants with LN. The cohort summary includes one control without a kidney myeloid IFN21 score.

eGFR, estimated glomerular filtration rate; CKD-EPI, Chronic Kidney Disease Epidemiology Collaboration; UPCR, urine protein-to-creatinine ratio.

Table S7B. Participant characteristics and IFN21

Outcome: donor-level kidney myeloid IFN21 score. Characteristic models include participants with LN and available data, regardless of genotype status.

Adjusted models include age per decade, sex, PC1–PC3 and log10 myeloid cell count, without duplicating the predictor of interest. Paired unadjusted and adjusted models use the same complete cases.

Characteristic / contrast	Model stage	N	β	CI lower	CI upper	Nominal P	BH q
Age per 10 years	Unadjusted available	155	0.016	-0.082	0.114	0.7432	0.8724
Age per 10 years	Unadjusted same complete cases	150	0.005	-0.095	0.105	0.9217	0.9756
Age per 10 years	Adjusted same complete cases	150	0.001	-0.106	0.108	0.9845	0.9845
Male versus female	Unadjusted available	155	0.169	-0.200	0.538	0.3675	0.4725
Male versus female	Unadjusted same complete cases	150	0.223	-0.149	0.595	0.2375	0.4008
Male versus female	Adjusted same complete cases	150	0.211	-0.166	0.589	0.2706	0.4297
Black or African American versus White	Unadjusted available	139	0.011	-0.270	0.292	0.9395	0.9756
Asian versus White	Unadjusted available	139	0.335	0.037	0.634	0.0278	0.2810
Black or African American versus White	Unadjusted same complete cases	134	-0.038	-0.323	0.246	0.7895	0.8882
Asian versus White	Unadjusted same complete cases	134	0.266	-0.034	0.567	0.0815	0.2810
Black or African American versus White	Adjusted same complete cases	134	0.236	-1.045	1.517	0.7160	0.8724
Asian versus White	Adjusted same complete cases	134	0.508	-0.016	1.031	0.0572	0.2810
Not Hispanic or Latino versus Hispanic or Latino	Unadjusted available	155	0.320	0.033	0.607	0.0292	0.2810
Not Hispanic or Latino versus Hispanic or Latino	Unadjusted same complete cases	150	0.273	-0.022	0.567	0.0692	0.2810
Not Hispanic or Latino versus Hispanic or Latino	Adjusted same complete cases	150	0.405	-0.007	0.817	0.0539	0.2810
Biopsy activity per point	Unadjusted available	89	0.014	-0.017	0.045	0.3623	0.4725
Biopsy activity per point	Unadjusted same complete cases	88	0.016	-0.016	0.047	0.3259	0.4725
Biopsy activity per point	Adjusted same complete cases	88	0.019	-0.023	0.061	0.3651	0.4725
Biopsy chronicity per point	Unadjusted available	88	-0.042	-0.111	0.028	0.2370	0.4008
Biopsy chronicity per point	Unadjusted same complete cases	87	-0.044	-0.113	0.026	0.2156	0.4008
Biopsy chronicity per point	Adjusted same complete cases	87	-0.056	-0.134	0.022	0.1593	0.3781
eGFR per 10 mL/min/1.73 m²	Unadjusted available	119	0.032	-0.005	0.069	0.0921	0.2810
eGFR per 10 mL/min/1.73 m²	Unadjusted same complete cases	118	0.033	-0.004	0.070	0.0825	0.2810
eGFR per 10 mL/min/1.73 m²	Adjusted same complete cases	118	0.039	-0.007	0.084	0.0937	0.2810
Proteinuria per doubling of UPCR	Unadjusted available	118	-0.089	-0.221	0.043	0.1820	0.3781
Proteinuria per doubling of UPCR	Unadjusted same complete cases	117	-0.092	-0.224	0.041	0.1724	0.3781
Proteinuria per doubling of UPCR	Adjusted same complete cases	117	-0.113	-0.253	0.027	0.1119	0.3021

P values are nominal. Benjamini–Hochberg (BH) q values account for all 27 characteristic coefficients across the three model stages.

Reported race and ethnicity are distinct from genetic ancestry principal components (PCs). eGFR is modeled per 10 mL/min/1.73 m²; proteinuria is modeled per doubling of UPCR.

Table S7C. Genotype and adjusted IFN21 models

C1 and C2 compare R77H carriers with non-carriers. Within each C1 analysis, all three adjustment stages use the same complete-case participants.

C1 R77H carrier versus non-carrier within LN

Analysis	Adjustment stage	N	Carriers	Non-carriers	β	CI lower	CI upper	Nominal P
Primary	Unadjusted	127	32	95	0.300	0.032	0.569	0.0288
Primary	Clinical and ancestry adjusted	127	32	95	0.339	0.054	0.623	0.0201
Primary	Additionally composition adjusted	127	32	95	0.300	0.015	0.585	0.0392
Renal covariates	Unadjusted	100	27	73	0.260	-0.045	0.565	0.0938
Renal covariates	Clinical and ancestry adjusted	100	27	73	0.346	0.051	0.641	0.0221
Renal covariates	Additionally composition adjusted	100	27	73	0.311	0.004	0.618	0.0474
Renal and biopsy covariates	Unadjusted	75	20	55	0.229	-0.143	0.602	0.2237
Renal and biopsy covariates	Clinical and ancestry adjusted	75	20	55	0.307	-0.060	0.674	0.0992
Renal and biopsy covariates	Additionally composition adjusted	75	20	55	0.256	-0.138	0.649	0.1989
Five ancestry PCs	Unadjusted	127	32	95	0.300	0.032	0.569	0.0288
Five ancestry PCs	Clinical and ancestry adjusted	127	32	95	0.349	0.072	0.626	0.0141
Five ancestry PCs	Additionally composition adjusted	127	32	95	0.306	0.034	0.579	0.0280
At least 20 myeloid cells	Unadjusted	109	30	79	0.236	-0.041	0.513	0.0946
At least 20 myeloid cells	Clinical and ancestry adjusted	109	30	79	0.282	-0.012	0.576	0.0596
At least 20 myeloid cells	Additionally composition adjusted	109	30	79	0.197	-0.092	0.485	0.1801

Clinical and ancestry covariates: age per decade, sex, PC1–PC3 and log10 myeloid cell count. Composition covariates: monocyte, granulocyte and dendritic/mast-cell fractions, with macrophages as the reference.

Renal covariates: eGFR and log2 UPCR. Biopsy covariates: activity and chronicity indices. Five-PC models include PC1–PC5. P values and 95% confidence intervals use HC3 robust standard errors and t tests.

C2 Before and after adjustment for rs3087796

Compartment / score scope	Covariates	N	Carriers	Non-carriers	β	CI lower	CI upper	Nominal P
Kidney bulk	PC1–PC5	127	32	95	0.339	0.097	0.580	0.0063
Kidney bulk	PC1–PC5 + rs3087796 dosage	127	32	95	0.314	0.067	0.562	0.0131
Kidney myeloid	PC1–PC5	127	32	95	0.345	0.072	0.619	0.0137
Kidney myeloid	PC1–PC5 + rs3087796 dosage	127	32	95	0.308	0.031	0.584	0.0296
Blood bulk	PC1–PC5	99	24	75	-0.243	-0.653	0.167	0.2421
Blood bulk	PC1–PC5 + rs3087796 dosage	99	24	75	-0.273	-0.693	0.146	0.1993
Blood myeloid	PC1–PC5	99	24	75	-0.260	-0.761	0.242	0.3068
Blood myeloid	PC1–PC5 + rs3087796 dosage	99	24	75	-0.283	-0.799	0.232	0.2780

C3 LN versus control in identical complete cases

Contrast	Adjustment stage	N	LN	Controls	β	CI lower	CI upper	Nominal P
LN versus control	Unadjusted	174	150	24	1.314	1.029	1.600	2.35E-16
LN versus control	+ clinical and ancestry	174	150	24	1.160	0.759	1.560	4.90E-08
LN versus control	+ myeloid composition	174	150	24	1.172	0.751	1.593	1.47E-07

The LN-versus-control models include 150 participants with LN and 24 controls, with identical complete cases across adjustment stages. Genotype availability is not an eligibility criterion.

Table S6. rs1143679 associations with IFN-related proteins after regulatory-marker adjustment

Table S8. Conformational-checkpoint protein class roster of 80 missense-led loci with trans-regulatory signatures

Gene	Lead variant	AA change	N trans targets	Autoimmune disease associated
ABCA7	rs3752246	G1527A	3	
ACKR2	rs2228467	V41A	9	
ARHGAP45	rs36084354	M515I	5	
ARHGEF3	rs3772219	L335V	4	
ATF7IP	rs3213764	K530R	8	
ATM	rs1801516	D1853N	15	
BANK1	rs10516487	R61H	3	Y
BANP	rs74992447	P356S	2	
BTN3A1	rs41266839	R282T	18	
CCM2	rs2107732	V53I	3	
CCR2	rs1799864	V64I	5	
CD226	rs763361	G307S	16	Y
CD300A	rs2272111	R111Q	3	
CTLA4	rs231775	T17A	2	Y
CX3CR1	rs3732378	T280M	38	
DCLRE1C	rs35441642	P171R	2	
DDX60L	rs61740720	R1387Q	3	
EIF2AK3	rs867529	S136C	4	
ERAP1	rs30187	K528R	3	Y
F5	rs6025	R534Q	2	Y
FASTKD1	rs12618227	E384Q	2	
FASTKD3	rs2966952	K56R	5	
FLACC1	rs13014235	V43L	2	
FLT3	rs1933437	T227M	2	
GGCX	rs699664	R325Q	7	
GSDMA	rs7212938	V128L	73	
GTF3C1	rs61739285	R1630H	2	
HFE	rs1800562	C282Y	18	
ICAM1	rs5498	K469E	2	
IFIH1	rs1990760	A946T	17	Y
IL6R	rs2228145	D358A	12	Y
ITGAM	rs1143679	R77H	2	Y
KLRC2	rs28403159	N2S	2	
KLRC4	rs2617170	N104S	44	Y
LACC1	rs3764147	I254V	2	Y
LRRC34	rs6793295	S249G	9	Y
LRWD1	rs148981077	P593L	2	
LTN1	rs34191159	G565C	2	
LY75	rs78446341	P1247L	4	
LYZ	rs1800973	T88N	17	
MKRN1	rs2272095	V243L	2	
MPO	rs56378716	M251T	13	
MS4A6A	rs7232	T185S	13	
NLRC5	rs74439742	P191L	4	
NPAT	rs34052882	N999K	2	
PFAS	rs4791641	P367L	2	
PML	rs5742915	F645L	2	
PTPN22	rs2476601	R620W	21	Y
RESF1	rs2166807	L250P	3	
REST	rs3796529	P797L	6	
RIN3	rs117068593	R279C	5	Y
RLIG1	rs9262	V238L	13	
RREB1	rs9379084	D1171N	19	
RRP12	rs1048445	R1281Q	4	
SERPINB10	rs8097425	I41M	8	
SH2B1	rs7498665	T484A	30	
SH2D3C	rs10760500	L23F	2	
SHARPIN	rs34173062	S17F	2	
SIRPB1	rs1535882	R23G	2	
SLC44A2	rs2288904	R154Q	7	Y
SLC5A6	rs1395	S481F	4	
SLFN12	rs2586514	C168R	3	
SWAP70	rs415895	Q505E	4	
TASOR	rs9835332	T1046R	3	
TASOR2	rs2275774	K2288R	11	
TBRG4	rs2304693	P57L	8	
THADA	rs7578597	T1187A	28	
TIRAP	rs8177399	R13W	4	
TMEM79	rs6684514	V147M	49	
TUBD1	rs1292053	M76T	18	Y
TYK2	rs34536443	P1104A	6	Y
WDFY4	rs7097397	R1816Q	10	Y
YBX3	rs1126501	T75A	2	
ZC3HC1	rs11556924	R363H	6	
ZNF28	rs10417163	K465Q	4	
ZNF485	rs45545532	R22W	2	
ZNF587B	rs35313547	V255A	6	
ZNF616	rs35582075	P50S	3	
ZSCAN5A	rs34187696	G337V	4	
ZXDC	rs16837497	P562L	4	

AA change follows GRCh38 reference->alternate HGVS. Where the current reference allele is the disease-associated residue, established clinical nomenclature is used instead (PTPN22 R620W, CD226 G307S, SLC44A2 R154Q).

N trans targets = distinct trans targets across evidence layers (eQTLGen discovery + replication, plasma pQTL, Koprulu pQTL); all class members have >=2. For genes with >1 qualifying missense variant, the maximum across variants is shown.

Table S7. AMP cohort characteristics and donor-level IFN21 associations.

Table S8. Conformational-checkpoint protein class roster of 80 missense-led loci with trans-regulatory signatures.

Supplementary References

1. Warmerdam CAR, et al. Trans-eQTLs reveal the architecture of human gene regulatory networks [preprint]. https://doi.org/10.64898/2026.02.04.26343575. Posted on medRxiv February 5, 2026.

2. Võsa U, et al. Large-scale cis- and trans-eQTL analyses identify thousands of genetic loci and polygenic scores that regulate blood gene expression. Nat Genet. 2021;53(9):1300–1310.

3. Yao Y, et al. Neutralization of interferon-α/β–inducible genes and downstream effect in a phase I trial of an anti–interferon-α monoclonal antibody in systemic lupus erythematosus. Arthritis Rheum. 2009;60(6):1785–1796.

4. The GTEx Consortium. The GTEx Consortium atlas of genetic regulatory effects across human tissues. Science. 2020;369(6509):1318–1330.

5. Koprulu M, et al. Multi-cohort proteogenomic analyses reveal genetic effects across the proteome and diseasome. Cell. 2026;189(11):3339–3357.e11.

6. The 1000 Genomes Project Consortium. A global reference for human genetic variation. Nature. 2015;526(7571):68–74.

7. Yazar S, et al. Single-cell eQTL mapping identifies cell type–specific genetic control of autoimmune disease. Science. 2022;376(6589):eabf3041.

8. Schmiedel BJ, et al. Impact of Genetic Polymorphisms on Human Immune Cell Gene Expression. Cell. 2018;175(6):1701–1715.e16.

9. Chen L, et al. Genetic Drivers of Epigenetic and Transcriptional Variation in Human Immune Cells. Cell. 2016;167(5):1398–1414.e24.

10. Sun BB, et al. Plasma proteomic associations with genetics and health in the UK Biobank. Nature. 2023;622(7982):329–338.

11. Uhlén M, et al. Tissue-based map of the human proteome. Science. 2015;347(6220):1260419.

12. Grantham R. Amino Acid Difference Formula to Help Explain Protein Evolution. Science. 1974;185(4154):862–864.

13. Cheng J, et al. Accurate proteome-wide missense variant effect prediction with AlphaMissense. Science. 2023;381(6664):eadg7492.

14. Hoover PJ, et al. Deep profiling of lupus nephritis kidneys reveals dynamic changes in myeloid cells associated with disease progression. Ann Rheum Dis. 2026;85(7):1324–1340.

15. He S, et al. High-plex imaging of RNA and proteins at subcellular resolution in fixed tissue by spatial molecular imaging. Nat Biotechnol. 2022;40(12):1794–1806.

16. Hao Y, et al. Dictionary learning for integrative, multimodal and scalable single-cell analysis. Nat Biotechnol. 2024;42(2):293–304.

17. Liberzon A, et al. The Molecular Signatures Database Hallmark Gene Set Collection. Cell Syst. 2015;1(6):417–425.

18. Faridi MH, et al. CD11b activation suppresses TLR-dependent inflammation and autoimmunity in systemic lupus erythematosus. J Clin Invest. 2017;127(4):1271–1283.

19. Han S, et al. Evaluation of imputation-based association in and around the integrin-α-M (ITGAM) gene and replication of robust association between a non-synonymous functional variant within ITGAM and systemic lupus erythematosus (SLE). Hum Mol Genet. 2009;18(6):1171–1180.

20. Fuss IJ, et al. Isolation of Whole Mononuclear Cells from Peripheral Blood and Cord Blood. Curr Protoc Immunol. 2009;85:7.1.1–7.1.8.

21. Lacey DC, et al. Defining GM-CSF– and Macrophage-CSF–Dependent Macrophage Responses by In Vitro Models. J Immunol. 2012;188(11):5752–5765.

22. Mia S, et al. An optimized Protocol for Human M2 Macrophages using M-CSF and IL-4/IL-10/TGF-β Yields a Dominant Immunosuppressive Phenotype. Scand J Immunol. 2014;79(5):305–314.

23. Coxon A, et al. A Novel Role for the β2 Integrin CD11b/CD18 in Neutrophil Apoptosis: A Homeostatic Mechanism in Inflammation. Immunity. 1996;5(6):653–666.

24. Martinez L, et al. A Genetic Model of Constitutively Active Integrin CD11b/CD18. J Immunol. 2020;205(9):2545–2553.

25. Yokogawa M, et al. Epicutaneous Application of Toll-like Receptor 7 Agonists Leads to Systemic Autoimmunity in Wild-Type Mice: A New Model of Systemic Lupus Erythematosus. Arthritis Rheumatol. 2014;66(3):694–706.

26. Villanueva V, et al. CD11b agonists offer a novel approach for treating lupus nephritis. Transl Res. 2022;245:41–54.

27. Ritchie ME, et al. limma powers differential expression analyses for RNA-sequencing and microarray studies. Nucleic Acids Res. 2015;43(7):e47.

28. Robinson MD, et al. edgeR: a Bioconductor package for differential expression analysis of digital gene expression data. Bioinformatics. 2010;26(1):139–140.

29. Astle WJ, et al. The Allelic Landscape of Human Blood Cell Trait Variation and Links to Common Complex Disease. Cell. 2016;167(5):1415–1429.e19.

30. Tajuddin SM, et al. Large-Scale Exome-wide Association Analysis Identifies Loci for White Blood Cell Traits and Pleiotropy with Immune-Mediated Diseases. Am J Hum Genet. 2016;99(1):22–39.

31. Vuckovic D, et al. The Polygenic and Monogenic Basis of Blood Traits and Diseases. Cell. 2020;182(5):1214–1231.e11.